Fall 12-21-2016

Activity Preservation of Plasmonic Biosensors with a Metal-Organic Framework

Lu Wang
Washington University in St. Louis

WASHINGTON UNIVERSITY IN ST. LOUIS

School of Engineering and Applied Science

Department of Mechanical Engineering and Materials Science

Thesis Examination Committee:
Srikanth Singamaneni, Chair
Guy M. Genin
Jeremiah J. Morrissey

Activity Preservation of Plasmonic Biosensors with a Metal-Organic Framework

by

Lu Wang

A thesis presented to the School of Engineering
of Washington University in St. Louis in partial fulfillment of the
requirements for the degree of
Master of Science

December 2016

Saint Louis, Missouri

Acknowledgments

This study is supported by the Soft Nanomaterials Laboratory at the Department of Mechanical Engineering and Materials Science. I would like to express my deepest appreciation to my advisor, Dr. Srikanth Singamaneni, for guiding this study, and for instructing me in how to become a professional researcher in many different aspects. I would like to thank Dr. Congzhou Wang for sharing his knowledge on this topic and providing suggestions on outlining research directions, designing experiments and organizing data throughout this project. I would like to thank Sirimuvva Tadepalli and Zheyu Wang for X-ray diffraction and transmission electron microscopy measurements. For their support, I would like to thank Qisheng Jiang, Keng-Ku Liu, Jingyi Luan and all the other members of the Soft Nanomaterials Laboratory.

I would like to thank all my committee members for their inspiring discussions and valuable inputs, which improved the structure and coherence of this study.

I would like to thank the Nano Research Facility (NRF) at Washington University for providing access to electron microscopy facilities.

I would also like to thank the Washington University School of Engineering and Applied Science for its scholarship towards my degree program.

Special thanks go to my parents, who have encouraged me to choose a career path in science and engineering since childhood, and supported me financially in seeking advanced degrees. I will keep working and continue to thrive in this field.

Lu Wang

Washington University in St. Louis

December 2016

Contents

List of Figures

List of Tables

ABSTRACT OF THE THESIS

Activity Preservation of Plasmonic Biosensors

with a Metal-Organic Framework

by

Lu Wang

Master of Science in Materials Science

Washington University in St. Louis, 2016

Research Advisor: Professor Srikanth Singamaneni

Antibody-antigen recognition enables antibody-conjugated nanostructures to serve as plasmonic biosensors with tunable specificity. However due to the instability of antibodies, these biosensors are susceptible to changes in the environment such as heat and aridity, leading to constraints on the transportation and handling of these sensors. Here we establish a method using a metal-organic framework crystal to preserve biosensor activity under severe environmental conditions, including exposure to high temperatures, an organic solvent and a proteolytic agent. After zeolitic imidazolate framework-8 (ZIF-8) crystals formed for 12 hours on a biosensor of gold nanorods conjugated with a model antibody, rabbit IgG, 80% of the antibody activity is successfully retained after incubation at 60 °C for 24 hours. We investigated the change of preservation ability with respect to the growth of ZIF-8 film. Furthermore, in comparison with silk fibroin films, which showed similar function in previous studies, ZIF-8 films demonstrate stronger preservation ability in various conditions.

Chapter 1

Background

Antibody-based plasmonic biosensors have been considered a powerful and cost-efficient sensing tool with potential applications in clinical and military settings [1]. The use of antibody-antigen recognition ensures high accuracy of sensing, and the plasmonic resonance of conjugated metal nanoparticles pushes the resolution and sensitivity of these sensors to the single-molecule level [1,2]. However, the nature of the antibody on these metal nanoparticles makes conjugated biosensors susceptible to changes in the environment such as temperature rise, leading to the loss of sensing capability in harsh conditions [3]. Successful preservation of the sensing activity would significantly expand potential applications of these biosensors. This chapter will review the fundamental science that led to this study of activity preservation for plasmonic biosensors.

1.1 Antibody-Antigen Recognition

Higher vertebrates can respond to the invasion of various foreign substances, including viruses, bacteria, or even molecules. This defense mechanism is known as immune response, and the foreign substances that can elicit immune responses are called antigens. Proteins that are generated by an organism and can adaptively bind to antigens are known as immunoglobulins, and the secreted immunoglobulins are called antibodies [4]. Each antibody monomer consists of four polypeptide chains that covalently form a Y-shape structure. The peptide chains are linked with disulfide bridges (-S-S- structures), and each tip of the Y shape possesses a specific binding site for the complementary antigen, as shown in Figure 1.1 [4,5].

Immunoglobulin G (IgG) is the most abundant group of antibodies in the human circulatory system, representing approximately 75% of serum antibodies [4]. Thus it is often used as a model antibody in immunology and diagnostics. When antibodies from one vertebrate are introduced into the circulation system of another species, they can also elicit immune responses as an antigen, and the new antibodies produced are known as secondary antibodies. Secondary antibodies are widely used for signal amplification in bioassays such as enzyme-linked immunosorbent assay (ELISA) and

immunoblotting [6,7]. In this study, rabbit IgG and its secondary antibody (anti-IgG) in goat are used as antibody-antigen pair for the model biosensor.

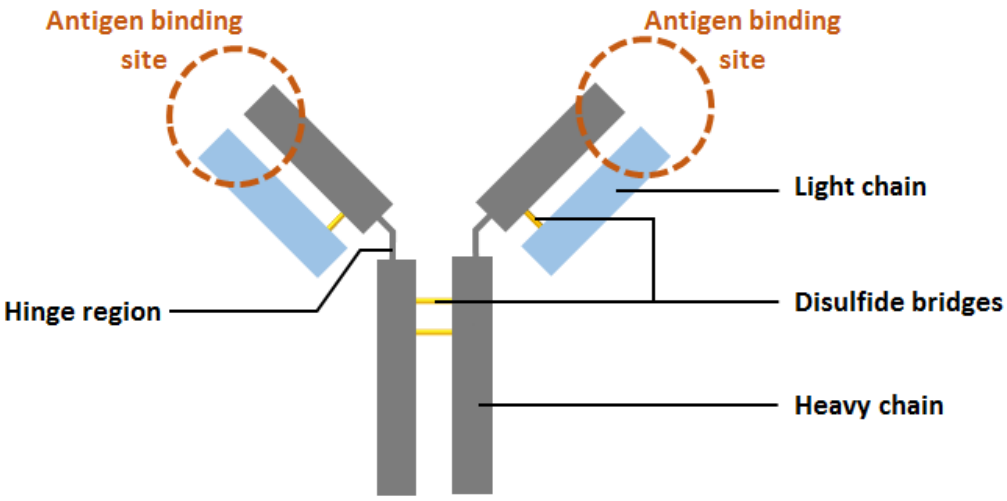

Figure 1.1 General structure of IgG, with different components and specific antigen binding sites labeled.

However, natural antibodies exhibit poor stability under change of pH, in nonaqueous media, at elevated temperature, and when exposed to proteolytic agents [8-10]. Thus despite their high accuracy and signal amplification potential, antibody-based biosensors have limited application due to their tendency to lose functionality in various conditions, especially at high temperatures. Therefore an extensive refrigerated distribution network, also known as a "cold chain", is often used to transport, store and handle antibody-based products [3]. This cold chain is expensive and heavily energy-consuming, and thus it greatly restricts the use of these biosensors in resource-limited areas, such as the developing countries and battle fields [11].

1.2 Localized Surface Plasmon Resonance

Surface plasmon resonance (SPR) is a coherent oscillation of the surface conduction electrons excited by electromagnetic radiation, e.g. light radiation [12]. Plasmonic materials, which are materials exhibiting this particular light-matter interaction, have been used in various applications in biological and chemical sensing [13,14]. In the case of localized surface plasmonic resonance (LSPR), a phenomenon widely observed in nanoscale metallic particles, light interacts with particles much smaller than its wavelength, leading to local oscillation of nanoparticles as shown in Figure 1.2. This local oscillation causes a change in the electric field of the incident light. The extent of this phenomenon is reflected in the extinction spectrum of light, which accounts for both absorption and scattering by the metal nanoparticles [12]. Extinction peak wavelengths largely depend on the size and shape of nanoparticles, and can be easily affected by the local changes in the dielectric environments. Therefore the extinction spectra of nanoparticles shifts due to adsorption of large molecules, such as polymers, on the particle surface [15,16]. By tuning the nanoparticle surface for specific adsorption of certain molecules, we can achieve chemical and biological sensing by analyzing the extinction spectra, which are typically obtained with an ultraviolet-visible (UV-vis) spectrometer.

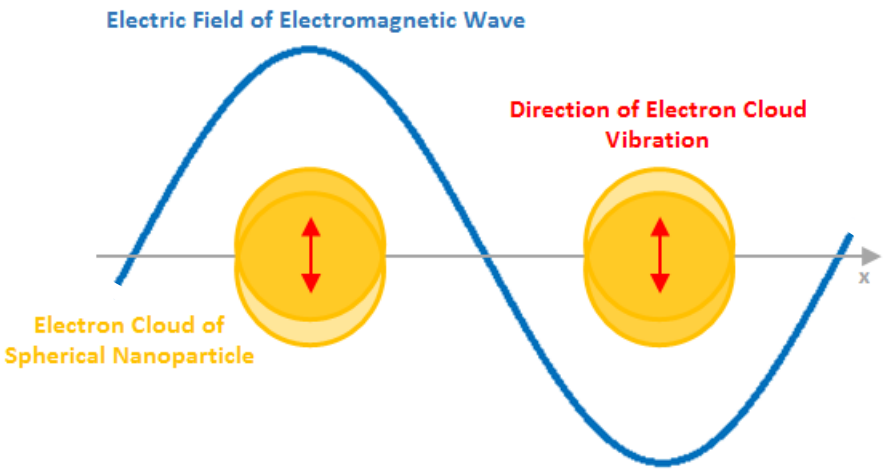

Figure 1.2 Localized surface plasmon resonance (LSPR) of spherical metal nanoparticles. Local vibration of nanoparticles causes a change in the electric field of the incident electromagnetic wave.

Among all metal nanoparticles, elongated gold nanorods (AuNRs) have shown great potential in plasmonic sensing considering that their LSPR wavelengths are easily tuned in large amounts by changing their overall size and forming sharp corners that function as electromagnetic hotspots [17-19]. When metal nanoparticles are not spherical, multiple extinction peaks result from the vibrational modes along different directions. In the case of an AuNR, the two most apparent extinction peaks can be attributed to the longitudinal and transverse dipole resonance, as shown in Figure 1.3. The peak positions are linearly dependent on the aspect ratio, which is the ratio between the longitudinal and transverse dimensions (length and diameter) [15]. For AuNRs with the same size and shape, the peak extinction values mainly depend on the concentration of particles, while the peak positions shall not change. In this study, AuNRs with average aspect ratio of around 4 were used to generate LSPR, with their largest peak position at around 810 nm in solution.

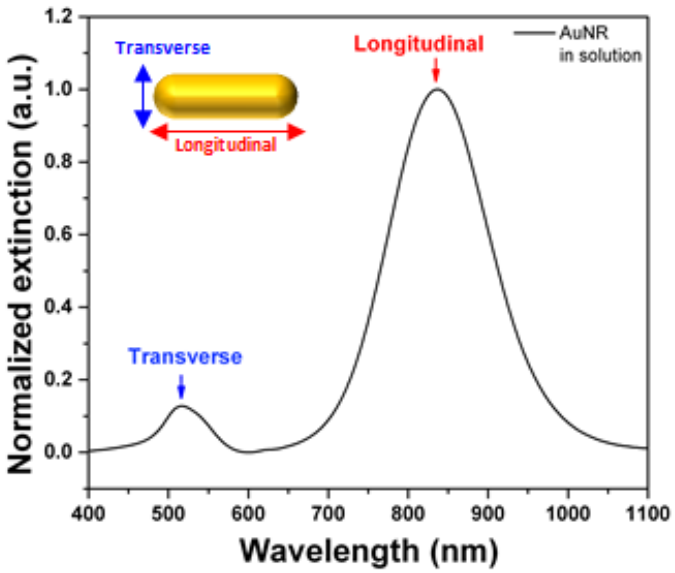

Figure 1.3 Example extinction spectrum of AuNRs in solution, with two LSPR peaks related to vibrational modes along different directions as illustrated.

1.3 Metal-Organic Framework

Metal-organic frameworks (MOFs) are inorganic-organic hybrid compounds that form microporous crystalline structures [19,20]. Their high surface areas and structural diversity allow these compounds to be applied in various fields such as gas separation and heterogeneous catalysis [22,24]. Among the MOFs, zeolitic imidazolate framework-8 (ZIF-8) is one composed of zinc ions and 2-methylimidazolate groups. Each zinc ion is coordinated by four methylimidazolate rings. ZIF-8 can form cubic crystals, or truncated octahedral crystals as shown in Figure 1.4. The ZIF-8 crystals are extremely stable in high heat and intrinsically biodegradable, making them an optimal material in biomedicine [22 – 25].

In previous studies, ZIF-8 has shown great potential in preserving the structural integrity and physiological function of biological macromolecules including proteins and deoxyribonucleic acids (DNAs) [25]. In an aqueous solution of zinc ions and 2-methylimidazole molecules, those biological macromolecules can efficiently induce the formation of ZIF-8 crystals on their surfaces. With a ZIF-8 protective layer, a model enzyme protein, horseradish peroxidase (HRP), can maintain its catalytic function under exposure to a proteolytic agent, high heat, and a boiling organic solvent [25]. The preservation mechanism is attributed to the small pore size of ZIF-8 and coordination interactions between the carbonyl groups of the protein backbone and the Zn cations of ZIF-8, providing proteins with tight encapsulation [25,26]. This led to our idea that ZIF-8 might also preserve the function of antibody-based plasmonic biosensors. However, HRP is reported with higher thermal stability than that of antibodies [8,27]. Moreover, activity of some antibodies could dramatically change when binding to a surface from an aqueous solution [28]. Antibodies conjugated on AuNRs are especially unstable, even when refrigerated at 4 °C [29]. Therefore, activity preservation is a greater challenge for plasmonic biosensors, which are built with antibodies tethered on the surfaces of metal nanoparticles.

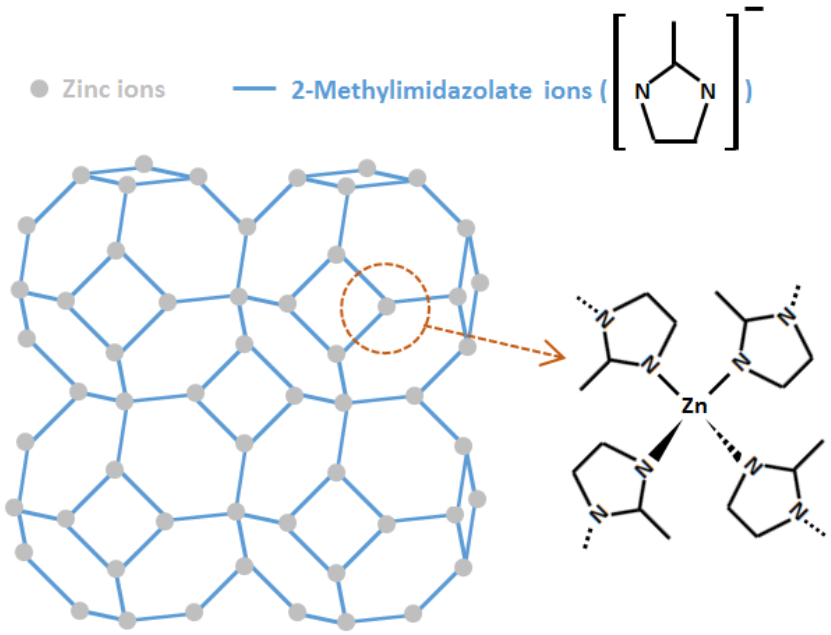

Figure 1.4 Truncated octahedral crystal structure of ZIF-8, the metal organic framework used in this study. Each zinc cation (gray dot) is linked with four nitrogen atoms in four 2-methylimidazolate residues (blue lines), together forming a crystal structure similar to zeolite crystals.

1.4 Silk Fibroin Film

Silk of domesticated silkworms (*Bombyx mori*) has been widely recognized for its strength and luster. The major component of *B. mori* silk is a protein called fibroin [30,31]. 94% of the silk fibroin amino acid sequence is composed of glycine-X (Gly-X) repeats, which then form β-sheet secondary structure with each other through hydrogen bonds. The strictly alternating Gly-X sequence allows the β-sheets to densely pack on one another via Gly/Gly or X/X contacts, which lead to the impressive mechanical strength of the *B. mori* silk [34]. The packed domains are also known as the crystalline domains of silk fibroin.

In recent years, silk fibroin has drawn great attention in the field of biomedicine, due to its biocompatibility, mechanical strength, cost-efficient extraction process and controllable degradation [30-33]. It has been widely applied in tissue engineering, wound healing, drug delivery and many other biomedical researches [33]. Previous studies have shown that silk fibroin film is a good candidate for preserving activity of plasmonic biosensors [35]. Therefore in this study, the preservation ability of silk fibroin film is discussed as a comparison.

1.5 Methodology Overview

This study focuses on the preservation of antibody-based plasmonic biosensors with a film made of ZIF-8 crystals. The plasmonic biosensors are constructed by conjugating IgG onto the surface of AuNRs, and further localizing this conjugated structure on glass slides. Using the antibody proteins as nucleation sites, ZIF-8 can form a rigid crystal layer on the surface of these plasmonic biosensors, as shown in Figure 1.5. This layer can later be easily removed by solution with low pH. Because ZIF-8 has high thermal stability, we proposed that by growing a film of ZIF-8 on the surface of antibody-based plasmonic sensors, the chemical structure of antibody proteins on the sensors can be retained under harsh conditions that would normally destroy the secondary interactions but not covalent bonds. This protection of structure integrity should lead to preservation of the sensing ability for these biosensors. This method, as illustrated in Figure 1.5, could potentially replace the expensive "cold chain" that is required for transportation of these biosensors.

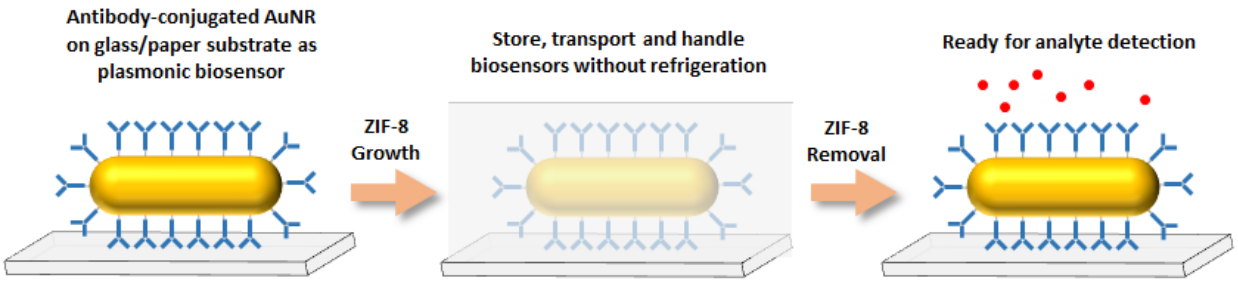

Figure 1.5 Method of activity preservation for antibody-based plasmonic biosensors proposed in this study. After ZIF-8 growth on biosensors, the biosensors retain their activity without refrigeration. Once ZIF-8 is removed, the biosensors should be ready to use.

We examine the stability of this proposed method for preserving biosensor activity under different conditions that would destroy the sensor function, including exposure to high temperatures (40 °C, 60 °C, 80 °C and 120 °C), an organic solvent (dimethylformamide) and a proteolytic agent (protease from *Streptomyces griseus*). The sensor function is characterized by the LSPR shift in its extinction spectrum. The outline of all experiments in this study is shown in Figure 1.6. Characterization of the biosensors surfaces is done with X-ray diffraction (XRD), transmission electron microscopy (TEM) and atomic force microscopy (AFM) between different steps. Preservation of the biosensor activity with silk film is explored as a comparative study.

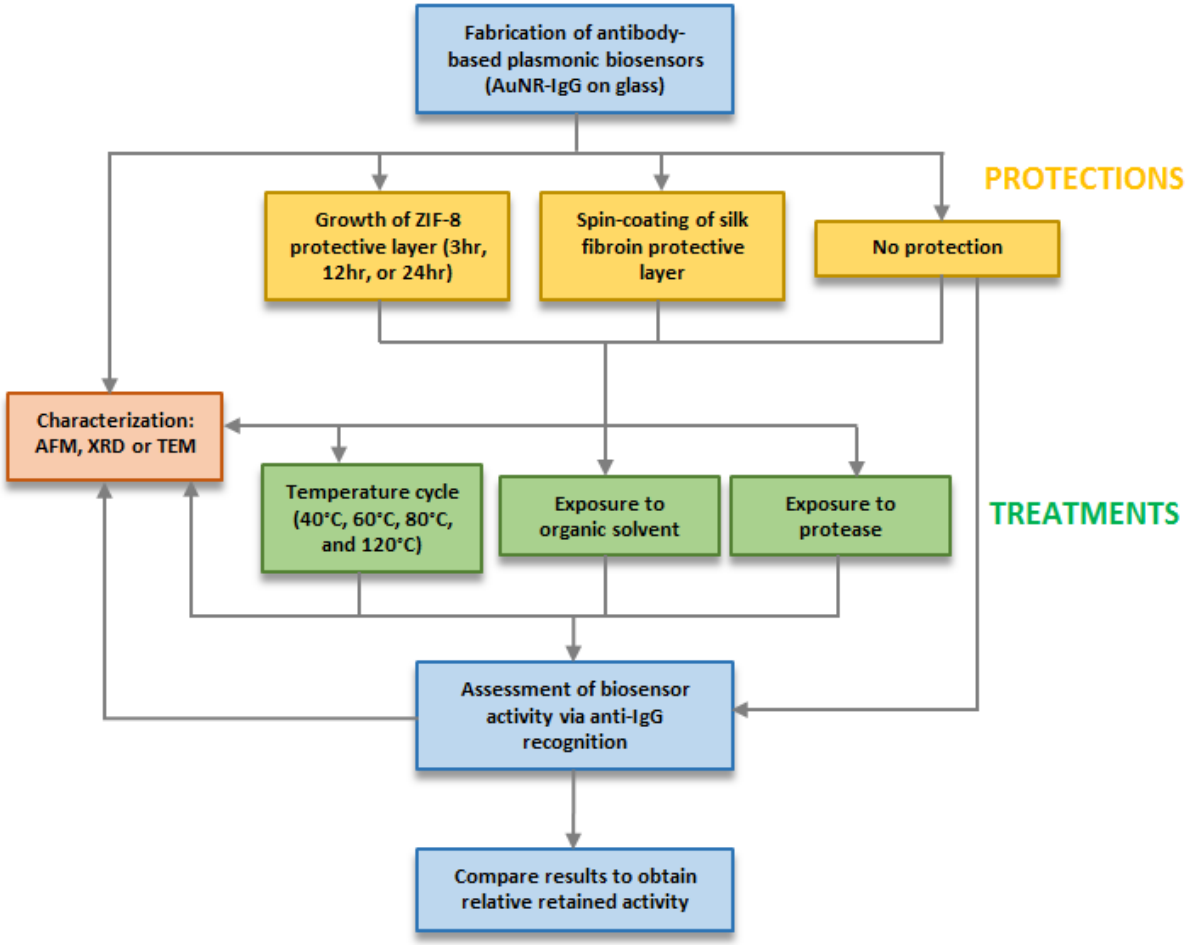

Figure 1.6 Procedure outline of experiments in this study. After fabrication of the biosensors and formation of the protective layers (ZIF-8 or silk films), the biosensors then go through treatments and their activities are assessed afterwards. Surface characterization techniques are used to further understand the interactions between protective layers and the biosensors surfaces.

Chapter 2

Methods

This chapter describes different techniques and methodologies used in this study. Here, plasmonic biosensors were fabricated by conjugating rabbit IgG on the surface of AuNRs, which were then localized on glass substrates. The recognition ability of rabbit IgG was shown by successful binding of its secondary antibody, goat anti-rabbit IgG. Each additional layer of protein on AuNRs causes a shift in their LSPR peaks. Therefore successful preservation of biosensing ability was shown by retained binding activity of IgG to anti-IgG, which can be studied by analyzing the extinction spectra of the plasmonic sensors. Various characterization techniques were also utilized to study the ZIF-8 film and silk fibroin film used in biopreservation.

2.1 Materials

Cetyltrimethylammonium bromide (CTAB), chloroauric acid ($AuCl_4$), sodium borohydride ($NaBH_4$), ascorbic acid, (3-mercaptopropyl)-triethoxy-silane (MPTES), zinc acetate dihydrate, 2-methylimimdazole, protease from *Streptomyces griseus* (Type XIV), dimethylformamide (DMF) potassium phosphate monobasic (KH_2PO_4), potassium phosphate dibasic (K_2HPO_4) and 10× phosphate buffer saline (PBS) were purchased from Sigma-Aldrich. Silver nitrate ($AgNO_3$) was purchased from VWR international. 1-Ethyl-3-(3-(dimethylamino)propyl) carbodiimide (EDC), N-hydroxysuccinimide (NHS), Rabbit IgG and Goat anti-Rabbit IgG (Mw = 150 kDa) were purchased from Thermo scientific. Poly(ethylene glycol) 2-mercaptoethyl ether acetic acid (SH-PEG-COOH, Mw = 5000g/mol) was purchased from Jenkem Technology. All chemicals were used as received, without further purification.

2.2 Fabrication of Antibody-Based Plasmonic Biosensors

Antibody-Based plasmonic biosensors are fabricated through three steps: synthesis of the gold nanorods (AuNRs), conjugation of IgG on AuNRs, and adsorption of AuNR-IgG conjugates on glass substrates. This section will introduce the fabrication of these plasmonic biosensors in detail.

2.2.1 Synthesis of Gold Nanorods

AuNRs were synthesized according to an established seed-mediated approach with some modifications [18,37]. All aqueous solutions in this procedure were prepared with nanopure water (18.2 MΩ cm). To prepare the seed solution for AuNR growth, 9.75 mL of 0.1 M CTAB and 0.25 mL of 10 mM $AuCl_4$ were mixed in an aqueous solution and kept under stirring at 800 rpm at room temperature. Then we prepared 10 mM $NaBH_4$ aqueous solution and stored it at 4 °C for more than 20 minutes. Once taken out of the refrigerator, 0.75 mL of ice-cold 10 mM $NaBH_4$ solution was rapidly injected into the mixture solution while the stirring continued. The resulting seed solution should show a brown color.

AuNR solution was made by mixing the following aqueous solutions in sequence: 38.0 mL of 0.1 M CTAB, 2.0 mL of 10 mM $HAuCl_4$, 0.40 ml of 10 mM $AgNO_3$, 0.22 mL of 0.1 M ascorbic acid and 48 μL of the seed solution. After adding each solution into a 50 mL centrifuge tube, we gently shook the centrifuge tube for 10 sec to ensure blending. Mixed solution was then completely covered with aluminum foil and left overnight for AuNR growth.

After observing a pink color in the AuNR solution, we stopped AuNR growth by centrifuging the solution at 8000 rpm for 20 min. The supernatant was discarded, and the precipitates were re-dispersed in nanopure water for storage. Extinction spectra of AuNR solution were obtained to monitor shape changes during the AuNR growth, and the amount of water added after centrifugation was controlled to ensure a longitudinal extinction peak value around 2.0. To remove excessive CTAB, the AuNR solution was centrifuged again at 8000 rpm for 20 min before usage.

2.2.2 Antibody Conjugation

The model antibody, IgG, was modified with SH-PEG-COOH and conjugated on AuNRs according to a previous study [16]. Aqueous solutions of 37.5 μL of 20 μM SH-PEG-COOH, 150 μL of 5 μM EDC, 60 μL of 12.5 μM NHS were mixed with 202.5 μL nanopure water and gently shaken for 1 hr. The pH of the reaction mixture was adjusted to 7.4 by adding 10× concentrated phosphate buffer saline (PBS). The mixture was then added with 10 μL of 75 μM IgG solution, and incubated at room temperature for 2 hr. The mixture was filtered using a centrifuge tube with a 50-kDa filter to remove any byproduct. The final SH-PEG-IgG conjugate solution was obtained after rinsing the mixture with PBS buffer (pH 7.4) twice through centrifuging at 7000 rpm for 5 min.

The IgG conjugated AuNR (AuNR-IgG) solution was prepared by adding 15 μL of SH-PEG-IgG solution to 1 mL of twice-centrifuged AuNR solution. The SH-PEG-IgG solution was added in smaller amounts (5μL) for multiple times, and the extinction spectrum of AuNR solution was checked after each addition to ensure successful conjugation. Successful conjugation was marked by a red shift of ~10 nm in the longitudinal peak of the extinction spectrum.

2.2.3 Adsorption of AuNR-IgG on Glass Substrates

Plasmonic biosensors were fabricated by adsorbing AuNR-IgG conjugates on glass substrates [35]. Glass substrates were cut into approximately 1 × 2 cm rectangular slides, and cleaned by immersing in piranha solution (3:1 (v/v) mixture of H_2SO_4 and 30% H_2O_2) for 40 min, followed by extensive rinsing with nanopure water. The clean glass substrates were then modified with MPTES for better adsorption of AuNR-IgG, by exposing their surfaces to 1% (m/v) MPTES in ethanol for 1 hr. Excessive MPTES was rinsed off by immersing the substrates in ethanol for 20 min, followed by extensive rinsing with nanopure water. The MPTES-modified glass substrates were then blow-dried and stored at 4 °C for at least 1 hr before use.

AuNR-IgG conjugates were adsorbed on glass substrates by exposing MPTES-modified glass substrates to AuNR-IgG solution for 1.5 hr at 4 °C. The adsorption time may increase to ensure a longitudinal extinction peak value of larger than 0.02. Excessive loosely-bound AuNR-IgG conjugates were rinsed off with nanopure water.

2.3 Formation of Protective Films

Protective films formed on top of the freshly fabricated plasmonic biosensors. Steps were performed immediately after one another to achieve maximum preservation.

2.3.1 ZIF-8 Protective Film

ZIF-8 protective film was constructed according to an established method [36]. To grow ZIF-8 protective film on a plasmonic biosensor, we placed the biosensor in a disposable cuvette. Precursor aqueous solutions of 80 mM 2-methylimidazole and 20 mM zinc acetate were prepared and slowly added onto the biosensor in sequence. After gently mixing the solution with a micropipet, we sealed the cuvette and soaked the biosensor in the mixture solution at 4 °C for 3 hr, 12 hr or 24 hr for ZIF-8 growth. The IgG molecules acted as nucleation centers for ZIF-8, and thus a film of ZIF-8 crystal grew on the biosensor. The ZIF-8 films can later be rinsed off with an aqueous solution of pH lower than 6. Here we used a potassium phosphate solution of pH 5.5.

2.3.2 Silk Protective Film

Silk fibroin was extracted in solution from *Bombyx mori* silkworm cocoons and used to form protective films following reported protocols [30,35]. To prepare the silk fibroin solution, *B. mori* cocoons were cut into small pieces (around 1 cm in diameter) and peeled into thinner sheets. Remains of the worm were carefully removed from the silk pieces. After boiling the silk pieces in 1 L of 0.02 M sodium carbonate aqueous solution, we obtained the dispersed silk fibroin fibers. The fibers were then removed with a spatula, rinsed with 1 L of nanopure water for 20 min three times, and dried overnight in a fume hood. Then we dissolved the dried fibers in 9.3 M lithium bromide (LiBr) at 60 °C for 4 hr, with a ratio of 1 g silk to 10 mL LiBr solution. The silk-LiBr solution was dialyzed with nanopure water in a capped dialysis tube (SnakeSkin 68700, Thermo Scientific) for 48 hr. We changed the water for dialysis six times within 48 hours. Then we removed the impurities in the dialyzed solution by centrifuging it twice at 9000 rpm at 4 °C, each time for 20 min. The supernatant was kept as the final silk fibroin solution and stored at 4 °C. The weight percentage of silk fibroin solution was determined by drying 200 μL of solution in a small weighing boat made

with aluminum foil (around 1 cm × 1 cm × 1 cm) at 60 °C, and weighing the dried film. The solution can later be diluted to lower concentrations.

To form the protective silk film, 120 μL of roughly 1% (m/v) silk solution was added onto the side of a plasmonic biosensor with AuNR-IgG, and spun-coated at 3000 rpm for 60 sec with a spin-coater (model WS-400, Laurell Technologies Corporation). The silk film can later be removed by gently shaking in nanopure water for 15 min.

2.4 Characterization

Characterization of AuNR extinction spectra and samples surfaces in this study was achieved through ultraviolet-visible (UV-vis) spectroscopy, X-ray diffraction (XRD), transmission electron microscopy (TEM) and atomic force spectroscopy (AFM).

2.4.1 Ultraviolet-Visible Spectroscopy

UV−vis extinction spectra of AuNRs were collected with a Shimadzu UV-1800 UV−vis spectrometer. For nanoparticle solutions, a minimum of 400 μL was transferred into a disposable cuvette for testing. For plasmonic biosensors on glass slides, a slide was inserted into a disposable cuvette, tilted for stable placement, and tested for the extinction spectra. Cuvettes with either nanopure water or clean glass tilted in the same orientation were used as baseline references for the spectrometer, thus the output extinction spectra should characterize the conjugated AuNRs and the protective layers. UV-vis spectra were analyzed with Origin software and the peak positions were determined by curve-fitting two Gaussian distributions.

2.4.2 X-ray Diffraction

The molecular composition of ZIF-8 crystals was verified with XRD. ZIF-8 was grown on a silicon substrate with AuNR-IgG adsorbed instead of a glass substrate following the same procedure in Section 2.4.1. The silicon substrates had been cleaned with piranha solution using the same procedure as cleaning glass slides in Section 2.2.3. The data were processed with Origin software.

2.4.3 Transmission Electron Microscopy

The sizes and shapes of AuNRs were verified through TEM. TEM graphs were collected and saved on a field emission microscope (JEOL JEM-2100F). Samples were prepared by drying a drop (~2 μL) of concentrated AuNR solution on a hydrophilic carbon-coated grid that had been processed by glow discharge. TEM images were analyzed with ImageJ 1.51h.

2.4.4 Atomic Force Microscopy

Surfaces of plasmonic sensors and protective films were characterized by AFM. An AFM image reflects relative height of a sample surface in bright or dark colors. We cooled the AFM samples to room temperature and blew dried samples to remove liquid and visible dust before scanning them with AFM. No other steps were taken for sample preparation. The images were obtained using Dimension 3000 (Digital instruments) AFM in light tapping mode. The tapping amplitude set point was varied until the sample surface was precisely captured. AFM images were processed with ImageJ 1.51h.

Thicknesses of protective films were also measured with AFM. A scratching tool with a sharp tip was used to create a step edge in the film on a glass sample. We carefully scratched the film so that the film was completely removed on the scratch site and that the glass substrate was not damaged. The area with the step edge of the film was examined with AFM in light tapping mode. The sample was oriented so that the scratch was on the top side, and perpendicular to the scanning direction of the AFM tip. The imaged area was selected so that no remains of the film could be seen at the bottom of the step, i.e. the bottom of the step was the top surface of the glass substrate. We obtained the average heights along the two sides of the step edge with the built-in software interface of the AFM machine. The film thickness was obtained from the average height difference between the top surface of the film and the top surface of the glass substrate. The data were processed with the software interface of Dimension 3000.

2.5 Activity Evaluation of Plasmonic Biosensors

The activity of an AuNR-IgG plasmonic biosensor was characterized by the peak shift in extinction spectra of AuNRs after binding of goat anti-rabbit IgG (anti-IgG). After removal of protection films on sensors surfaces, this binding is achieved by exposing the side with AuNR-IgG on a plasmonic biosensor to anti-IgG solution (diluted in 1× PBS buffer to 24 μg/mL) at 4 °C for 2 hr. The extinction peak values after binding of anti-IgG on sensors were obtained following the same procedure described in Section 2.4.1.

Within each batch of plasmonic biosensors, one or two samples were used as the internal references for this batch. The internal references were neither protected nor exposed to harsh environment, and they were directly exposed to anti-IgG to obtain the reference LSPR peak shift. If two samples were used as reference for the sample batch, we then set the average of the two peak shifts to be the reference value. All data were analyzed with Microsoft Excel and Origin.

2.6 Treatments on Plasmonic Biosensors

After protection film formed on the surface, the plasmonic biosensors experienced one of the following harsh environments. The internal references for every batch of plasmonic biosensors did not undergo any of these treatments.

2.6.1 Temperature Cycles

The plasmonic biosensors were placed in a glass or polystyrene petri-dish, with the side of AuNR-IgG facing top. The petri dishes were marked so that biosensors could be distinguished, and then placed into an oven preset to 40 °C, 60 °C, 80 °C or 120 °C for 24 hr. A glass petri dish was used for 80 °C and 120 °C cycles. After temperature cycles, the protective films were rinsed off right before activity evaluation of the biosensors.

2.6.2 Organic Solvent

Dimethylformamide (DMF) was used as to explore the effect of organic solvents on activity of plasmonic biosensors. A plasmonic biosensor was placed in a glass vial with ~10 mL of DMF for 2 hr, with the side of AuNR-IgG facing top. We ensured that the glass vials were sealed and that all biosensors were completely soaked during the treatment. We gently rinsed the plasmonic biosensors with nanopure water after taking them out of DMF.

2.6.3 Proteolytic Agent

Protease from *Streptomyces griseus* (Type XIV) was dissolved in 1× PBS to 0.25 units/mL. The plasmonic biosensors were placed in a petri dish with the side of AuNR-IgG facing top, and 150 μL of the protease solution was added onto each plasmonic biosensor. The petri dish was then sealed and placed at 37 °C for 2 hr statically in an incubator (Labnet International 311DS). The biosensors were gently rinsed with nanopure water after the incubation ended.

Chapter 3

Results and Analysis

Activity of an AuNR-IgG plasmonic biosensor was characterized by the peak shift in extinction spectra of AuNRs after binding of anti-IgG. By comparing the peak shift after incubation in harsh environment with the peak shift of intact reference biosensors prepared in the same batch, we obtained the percentage retained activity. Comparison of retained activities illustrated whether the protective films had successfully preserved the activity of plasmonic biosensors. Characterization of samples can also correlate the preservation ability of ZIF-8 film with its progressive growth.

3.1 Antibody-Based Plasmonic Biosensors

To study the function of plasmonic biosensors, we first verified the shape of AuNRs used in this study through TEM, as illustrated in Figure 3.1.

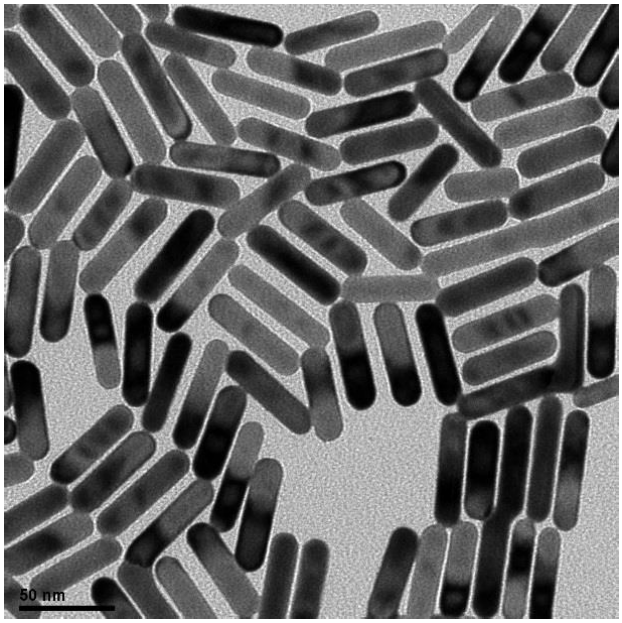

Figure 3.1 TEM image of AuNRs used in this study, with average aspect ratio of 3.9.

The length and diameter of these AuNR were found to be 54.5 ± 6.2 nm and 14.2 ± 1.7 nm respectively (N=30), and the average aspect ratio was calculated to be 3.9. These AuNRs showed extinction spectra with longitudinal peaks at ~830 nm in solution.

Conjugation of IgG on AuNRs was performed by adding SH-PEG-IgG solution into twice-centrifuged AuNRs solution in a cuvette several times. Every time, we added 5 μL of SH-PEG-IgG solution and checked the extinction spectrum of the result solution. Nanopure water was used as baseline reference for extinction spectra. After we added a total 15 μL of SH-PEG-IgG solution into the AuNR solution, there was a distinct red shift of ~9.2 nm in the longitudinal extinction peak (Figure 3.2), indicating successful conjugation of IgG onto the AuNRs.

After adsorbing AuNR-IgG conjugates on glass substrates, we also checked the extinction spectra of the fabricated plasmonic biosensors. A glass substrate previously cleaned with piranha solution was used as the baseline reference for the spectrometer. The longitudinal extinction peak was at ~790 nm, showing a blue shift compared to the extinction spectrum of AuNR-IgG solution.

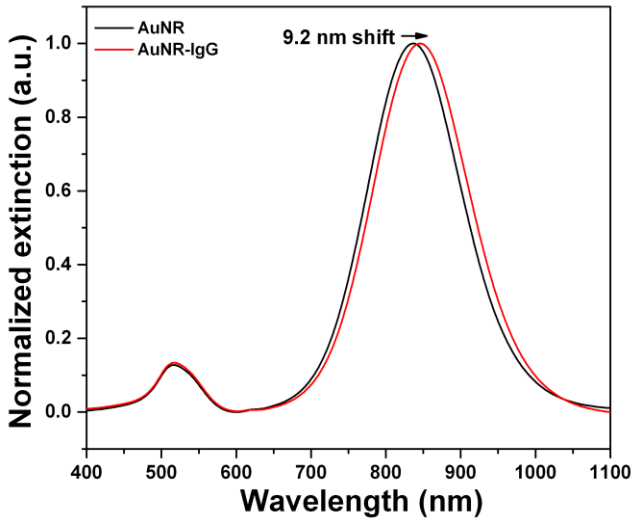

Figure 3.2 LSPR shift of AuNR solution after conjugation of rabbit IgG. An apparent shift of 9.2 nm in the longitudinal peak position is shown.

We then checked the morphologies of AuNR-IgG conjugates by scanning the surface of a fabricated plasmonic biosensor with AFM, as shown in Figure 3.3. Since AFM reads the relative height of sample surface, the bright and dark color should outline the size of the particles. We observed that the shape of AuNRs had changed into dumbbells after IgG conjugation. A few spherical particles

were observed. The AFM images showed uniform adsorption of AuNR-IgG conjugates on the glass substrates.

We verified the functionality of plasmonic biosensors through UV-vis spectroscopy. After exposure to anti-IgG solution, the plasmonic biosensors showed a roughly 30-nm red shift in the longitudinal extinction, as shown in Figure 3.4. This is quite significant compared to the 9.2-nm shift associated with IgG conjugation.

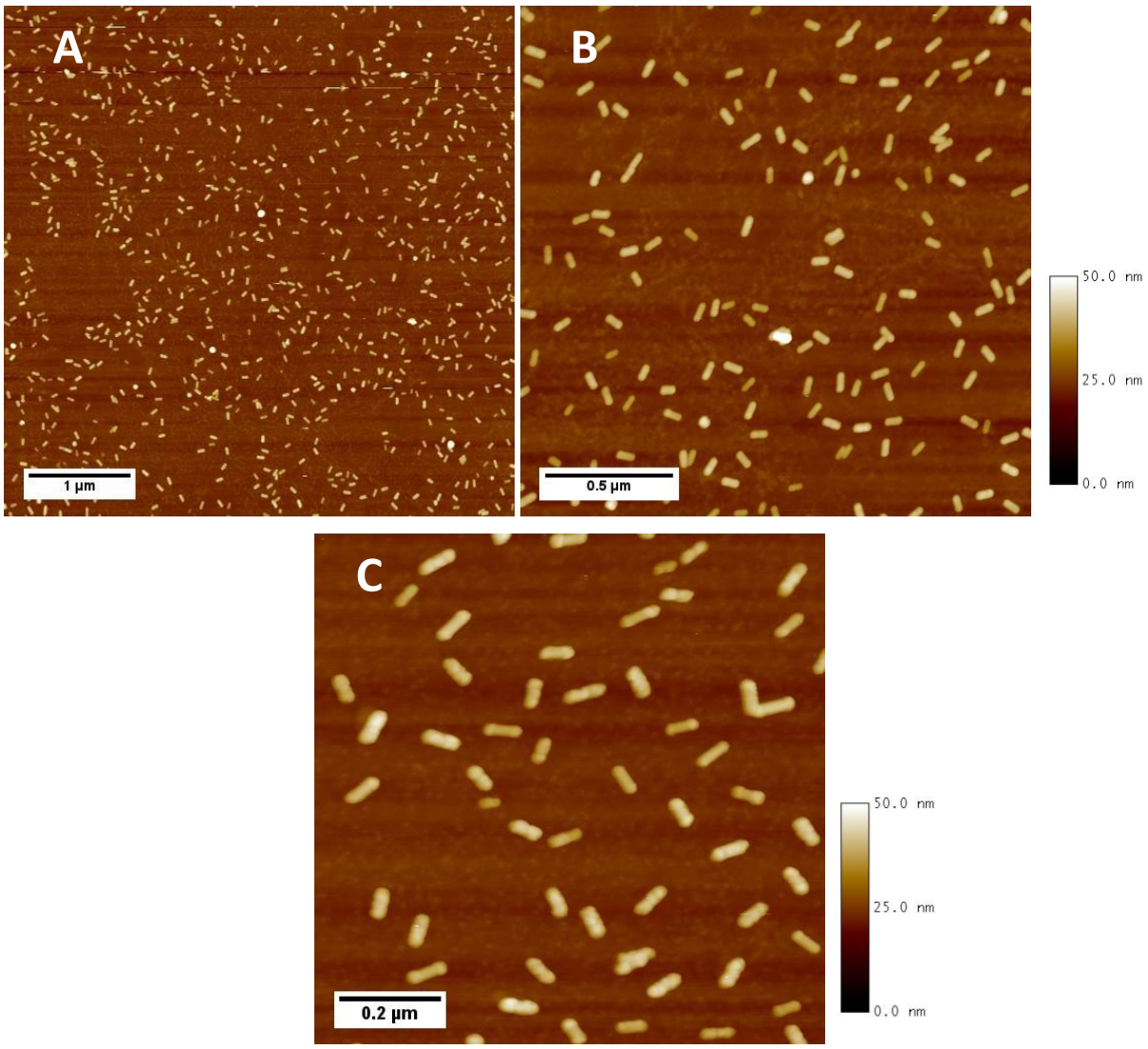

Figure 3.3 AFM images of AuNR-IgG conjugates after adsorption onto glass substrates. Three sizes of scans are shown (A: 5×5 µm, B: 2×2 µm, C: 1×1 µm).

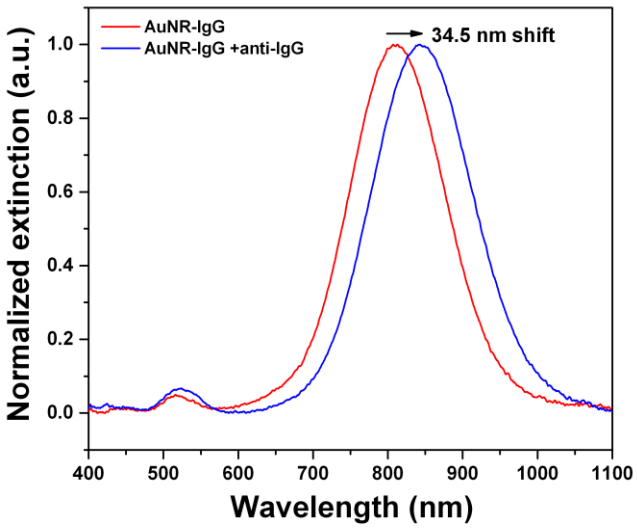

Figure 3.4 Example of LSPR shift of AuNR-IgG after exposure to anti-IgG solution (24 μg/mL) at 4 °C for 2 hr.

To explore the impact of ZIF-8 growth on the function of plasmonic biosensors, we explored how the extinction spectra changes after growth and removal of ZIF-8, as shown in Figure 3.5. Relative peak shifts were displayed in Figure 3.6. Upon formation of ZIF-8, the longitudinal extinction peak showed a red shift of 90 nm. The blue shift associated with removal of ZIF-8 is slightly larger than the previous red shift, which probably comes from the removal of some loosely-bound IgG. After removal of ZIF-8, the blue shift associated with binding of anti-IgG was ~30 nm, similar to previous observations with intact plasmonic biosensors.

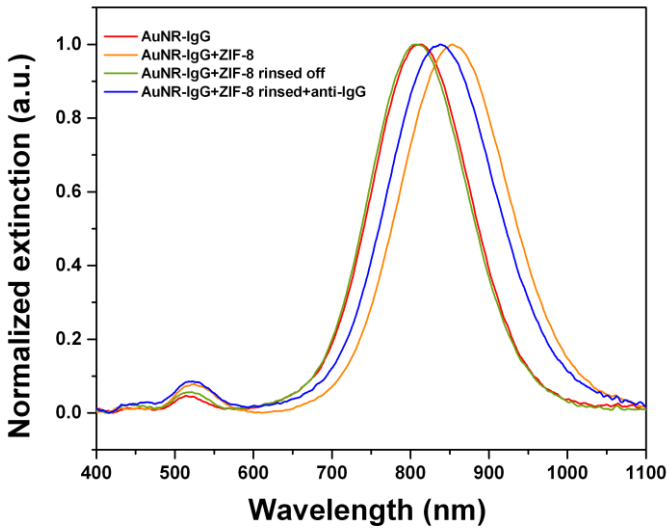

Figure 3.5 Extinction spectra of a plasmonic biosensor after 3-hr growth of ZIF-8 crystals, rinsing of ZIF-8 and anti-IgG binding.

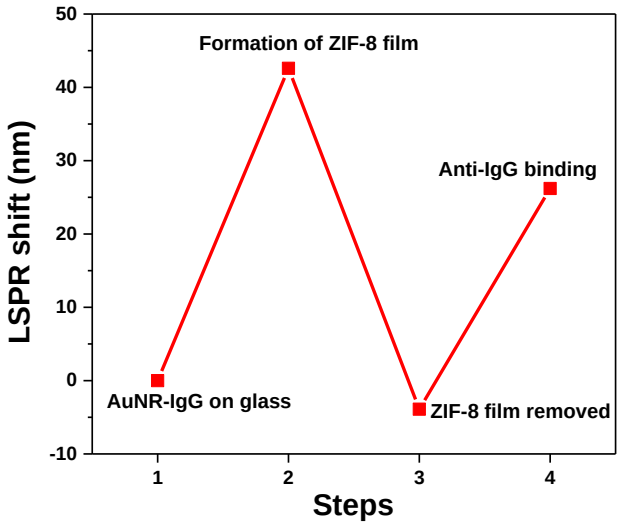

Figure 3.6 Typical LSPR shifts observed after 3-hr growth of ZIF-8 crystals, rinsing of ZIF-8 and anti-IgG binding.

We also checked the morphologies of AuNR-IgG conjugates after ZIF-8 growth and rinsing. After 12 hr of ZIF-8 growth, we rinsed off the ZIF-8 crystals on a plasmonic biosensor, and scanned its surface with AFM. The results are shown in Figure 3.7. Comparing these AFM images to Figure 3.3, we can see that the distribution of AuNR-IgG conjugates remained uniform after ZIF-8 growth. The overall shape and size of AuNR-IgG conjugates also did not change.

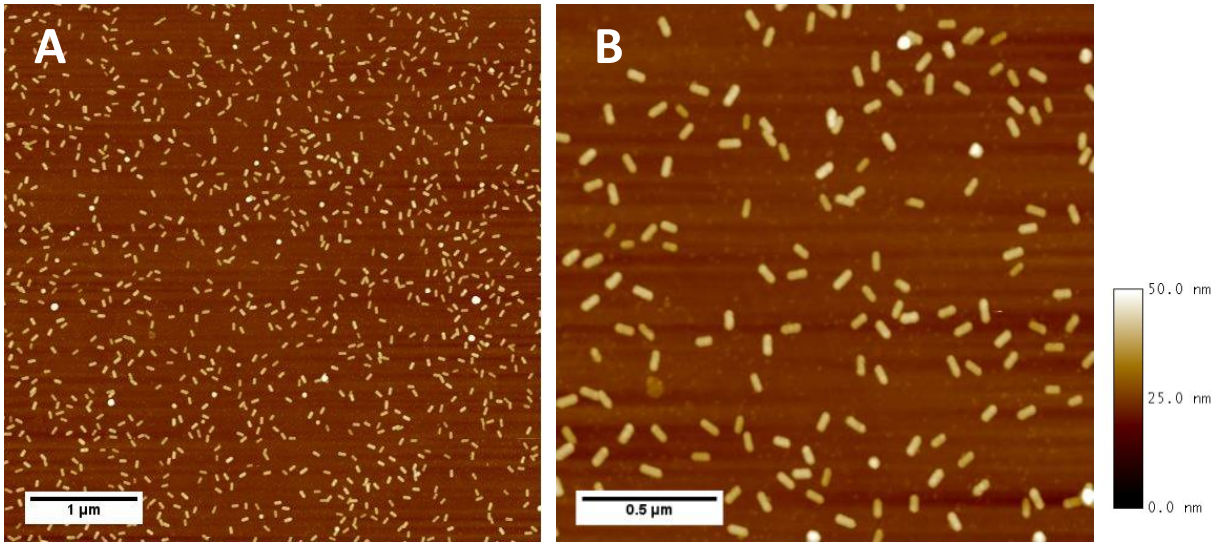

Figure 3.7 AFM images of AuNR-IgG conjugates after 12-hr ZIF-8 growth and rinsing of ZIF-8. Two sizes of scan are shown (A: 5×5 μm, B: 2×2 μm).

3.2 Activity Preservation at Elevated Temperatures

In each batch of plasmonic biosensors fabricated, we saved one or two sensors as the internal reference. We characterized the activity of a plasmonic biosensor by the red shift of its longitudinal peak position after anti-IgG binding. Therefore retained activity of a sample biosensor is calculated with the following equation:

$$\textbf{\textit{Retained activity}} = \frac{\textbf{\textit{Sample LSPR shift}}}{\textbf{\textit{Reference LSPR shift}}} \times \mathbf{100\%} \qquad \textbf{(3.1)}$$

Note that the sample and reference always came from the same batch.

After formation of ZIF-8 films for 3 hr, the protected plasmonic biosensors were incubated at different elevated temperatures for 24 hr, and the retained activities were assessed after the temperature treatment and removal of ZIF-8 films. A minimum of four samples were used for the

average of retained activity. We observed that these biosensors retained around 80% of their activity after removal of ZIF-8 films, at both 40 °C and 60 °C. At 80 °C, the average retained activity was 60%. Still it is significant compared to that of biosensors without ZIF-8 protection, as shown in Figure 3.8. The differences between protected and non-protected biosensor activities for all temperatures were larger than 50%.

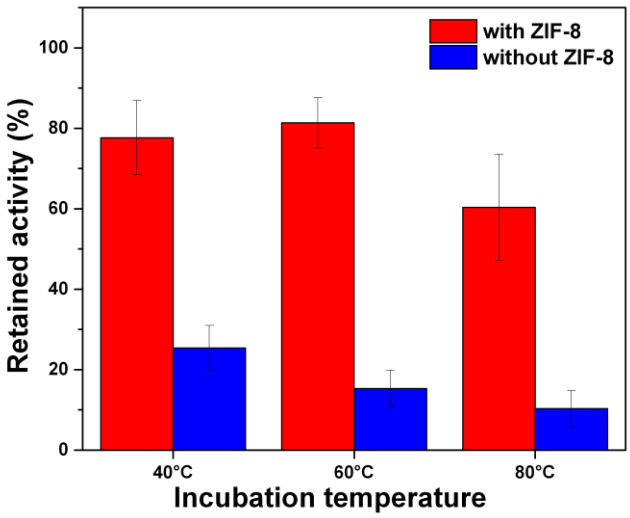

Figure 3.8 Retained activities of plasmonic biosensors after 24-hr incubation at elevated temperatures, with or without ZIF-8 protection (N ≥ 4 for each group). In the groups with ZIF-8 protection, biosensors were soaked in precursor solutions for 3 hours for ZIF-8 growth.

3.3 Progressive Growth of ZIF-8 Film

To understand the relationship between ZIF-8 crystal growth and its activity preservation function, we applied several characterization techniques on the ZIF-8 films. XRD was performed on ZIF-8 grown on AuNR-IgG conjugates adsorbed on silicon substrates, with the same procedure of growing ZIF-8 on plasmonic biosensors described in Section 2.3.1. In a crystal, XRD peaks can be associated with the crystal planes. Therefore we compared the XRD pattern (Figure 3.9) with the characteristic XRD peaks for freestanding ZIF-8 crystals [38]. The crystal planes corresponding to XRD peaks that we obtained are marked in Figure 3.9.

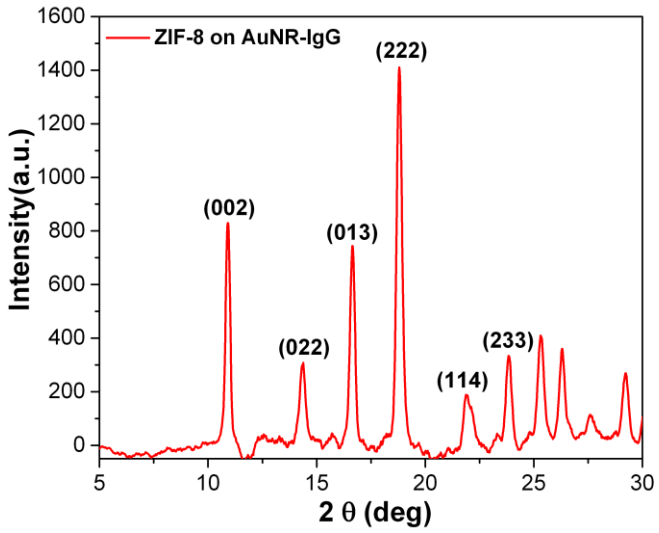

Figure 3.9 XRD data of ZIF-8 on AuNR-IgG. Peaks associated with crystal planes in pure ZIF-8 crystal are marked.

AFM was used in tapping mode to characterize the surface morphology of progressively growing ZIF-8. By directly testing the ZIF-8 on plasmonic sensors, we obtained Figure 3.10 for different ZIF-8 growth time: 3, 12 and 24 hours. For all three different growth times, the ZIF-8 formed a uniform film of crystal on top of the plasmonic sensors. No AuNR-IgG could be observed on the surface. Comparing these images, we can see that the size of ZIF-8 particles on surface increases with the growth time.

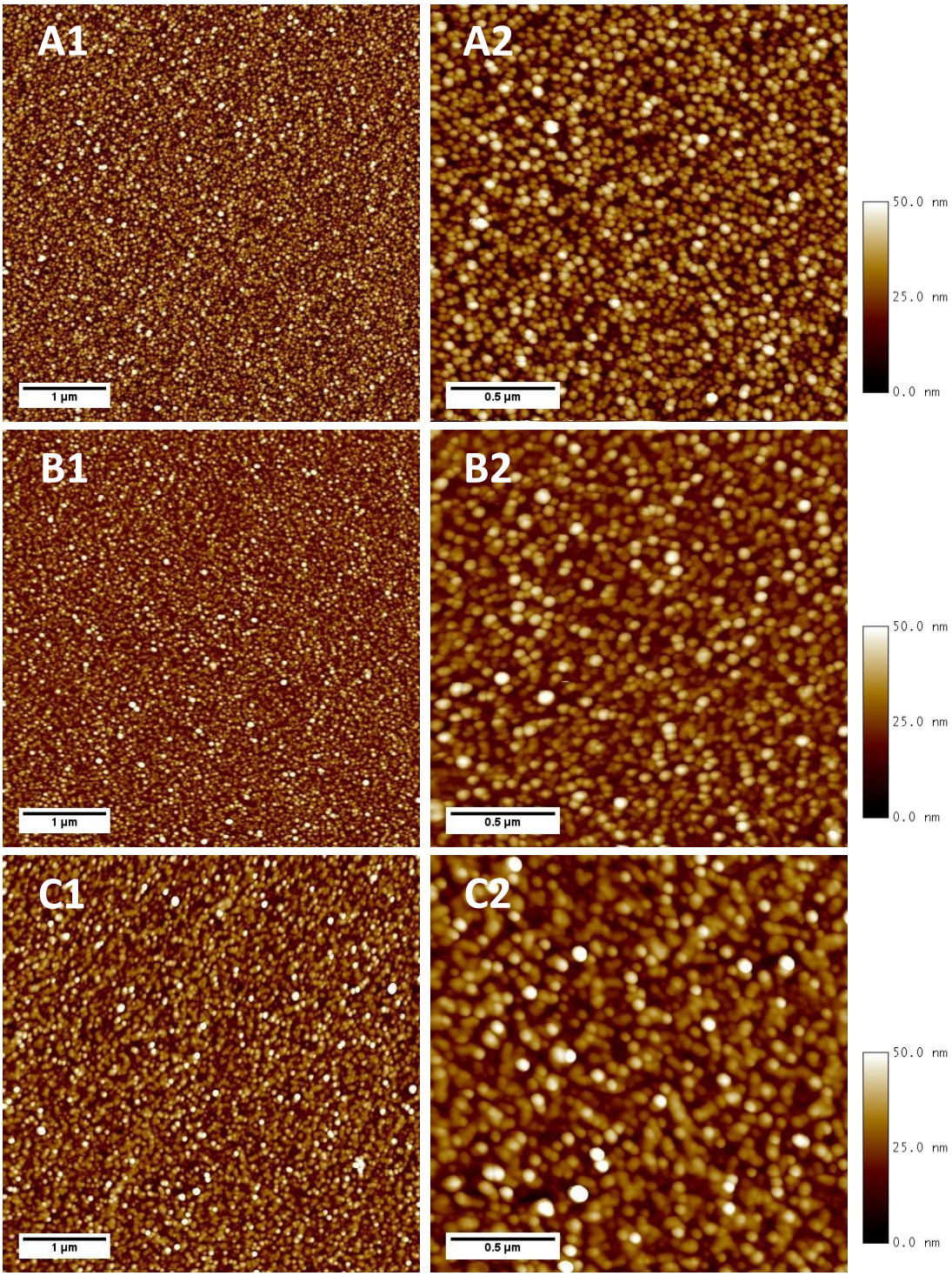

Figure 3.10 AFM images of ZIF-8 Film on AuNR-IgG after different growth times (A1, A2: 3 hr; B1, B2: 12 hr; C1, C2: 24 hr).

We also performed scratch tests on samples with different ZIF-8 growth times to study the films thicknesses. The images were obtained with AFM, as shown in Figures 3.11. After AFM images were flattened, the film thicknesses were obtained from the average height difference between the two sides of a scratch edge. In the black boxes on the AFM images in Figures 3.11, heights were averaged over the length of the box. The red lines indicate the data points selected for obtaining the average height on each side of the scratch edge. These red lines were carefully chosen to avoid shattered pieces of ZIF-8 film, which would cause deviations in the height readings. The average height profiles are shown in the yellow boxes on the right of AFM images in Figures 3.11. The range of x-axis of plot in the yellow box corresponds to the width of black box in AFM images, and the red arrows point at the values averaged from the red lines. The difference between values highlighted by the red arrows on the same AFM image was recorded as the ZIF-8 film thickness, as shown in Table 3.1.

Table 3.1 ZIF-8 film thicknesses after different growth times.

ZIF-8 Growth Time	Average Film Thickness
3 Hours	13.4 nm
12 Hours	16.4 nm
24 Hours	19.3 nm

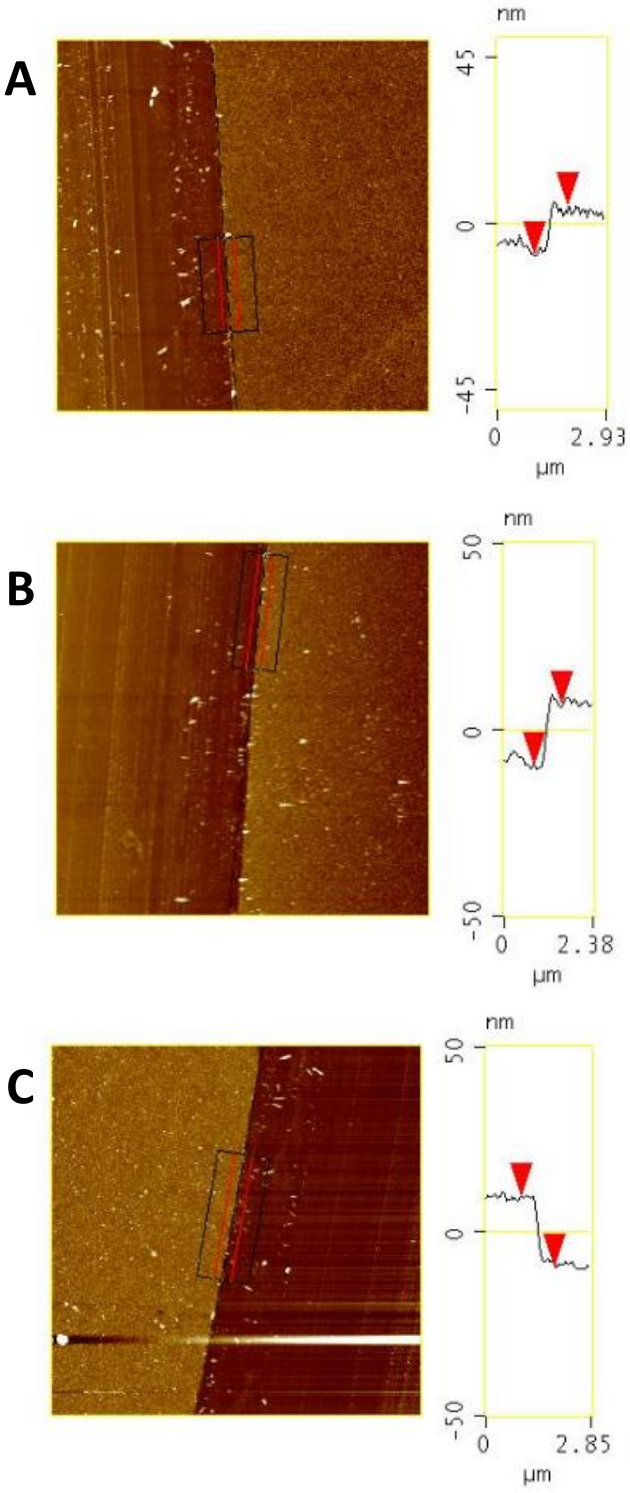

Figures 3.11 Thickness analysis of ZIF-8 films on AuNR-IgG after different growth times (A: 3 hr, B: 12 hr, C: 24 hr). Film edge regions are marked with black boxes. Height profiles along short sides of black boxes are plotted on the right of AFM scans in the yellow boxes. Red lines and arrows highlight the points selected for calculating average heights, which is later used for thickness calculation.

We also studied the effect of growth time of a ZIF-8 film on its preservation ability. After ZIF-8 growth on plasmonic sensors for different amounts of time (3 hr, 12 hr and 24 hr), the samples were incubated at 80 °C for 24 hours. The retained activity was calculated for each of the growth times, as shown in Figure 3.12. Without ZIF-8 protection, 10% of the biosensing activity was retained. The average retained activity increased to 60%, 76% and 78% after ZIF-8 growth for 3 hr, 12 hr and 24 hr, respectively. The retained activity clearly increases with the ZIF-8 growth time.

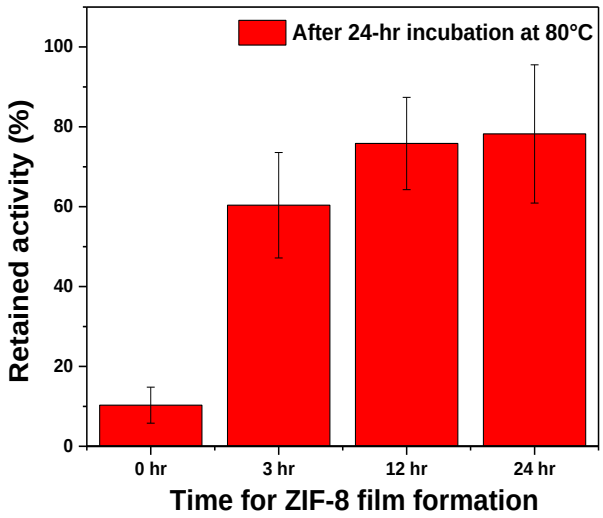

Figure 3.12 Change in preservation ability of ZIF-8 film with different growth time after incubation at 80 °C for 24 hr (N ≥ 4 for each group).

As a comparison, we also investigated the preservation of biosensor activity with silk fibroin film at 80 °C after 24 hr. The extinction spectra and LSPR shifts of a typical biosensor sample are shown in Figure 3.13 and Figure 3.14. These two figures show that the spin-coating of silk fibroin film on AuNR-IgG caused a red shift of ~120 nm. However after incubation of the samples at 80 °C and rinsing the silk with nanopure water, the blue shift of longitudinal peak associated with rinsing was only ~60 nm, indicating that the silk was not completely rinsed off. No anti-IgG binding was observed through LSPR shifts in the following step.

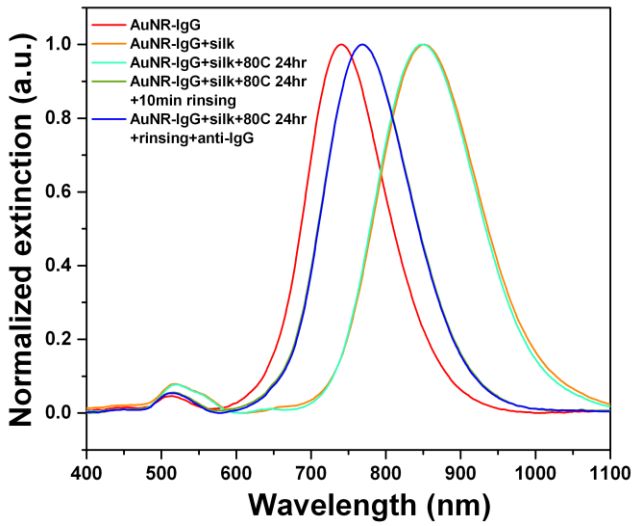

Figure 3.13 Extinction spectra of a plasmonic biosensor protected with silk fibroin films after silk film deposition, incubation at 80 °C for 24 hr, rinsing of silk and anti-IgG binding. The curve in dark green overlaps with that in blue.

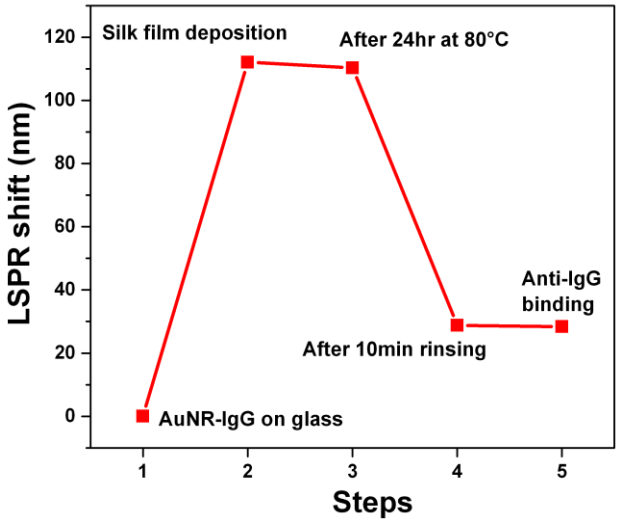

Figure 3.14 LSPR shifts of a plasmonic biosensor protected with silk fibroin films after silk film deposition, incubation at 80 °C for 24 hr, rinsing of silk and anti-IgG binding.

3.4 Activity Preservation at Extremely High Temperature

We also examined the activity preservation of ZIF-8 at an extremely high temperature (120 °C). After 12-hr ZIF-8 growth, incubation at 120 °C for 24 hr, and rinsing of ZIF-8 films, we obtained the extinction spectrum of a biosensor (Figure 3.15). The longitudinal peak showed a 20-nm blue shift compared to the original extinction spectrum of AuNR-IgG before the high temperature treatment. This is a much larger shift than that shown in Figures 3.5 and 3.6. This large blue shift indicates a change in the AuNR-IgG conjugates, and thus failure of the plasmonic biosensor. In this case, the peak shift from anti-IgG binding is not comparable to the reference shift anymore, indicating failure of the biosensors.

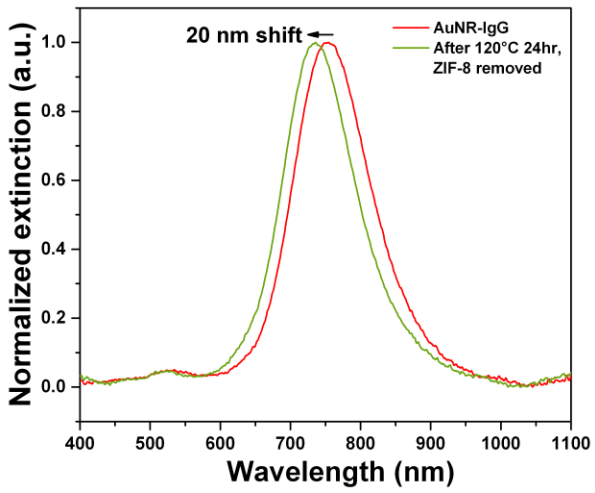

Figure 3.15 Extinction spectra of a plasmonic biosensor before and after 24-hr incubation at 120 °C plus rinsing of ZIF-8. ZIF-8 grew on the biosensor surface for 12 hr.

To further study what happened to these biosensors, we scanned the surfaces of ZIF-8 protected biosensors with AFM after incubation at 120 °C for 48 hr (Figure 3.16) and after removal of ZIF-8 (Figure 3.17). The ZIF-8 grew for 12 hr on the biosensors surfaces. Comparing Figure 3.16 to Figure 3.10-B2, the ZIF-8 crystals did not show a substantial morphology change after incubation at 120 °C. We can still observe clearly defined round crystals in Figure 3.16, and the ZIF-8 coverage is still uniform. However as we removed the ZIF-8 layer, we can clearly see deformed AuNR-IgG in

AFM images, as circled in red in Figure 3.17. The general size and shape of AuNR-IgG in Figure 3.17 are also not as uniform as that shown in Figure 3.3.

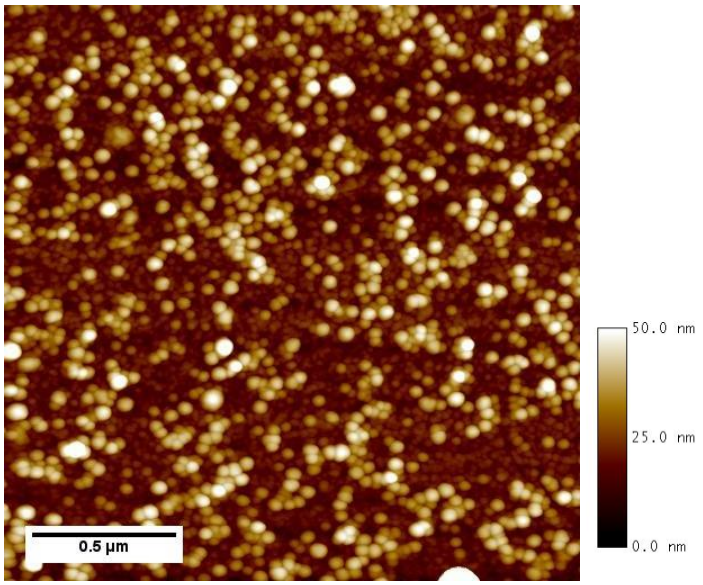

Figure 3.16 AFM image of ZIF-8 on AuNR-IgG after 48-hr incubation at 120 °C, showing uniform coverage of ZIF-8. ZIF-8 grew on the biosensor surface for 12 hr.

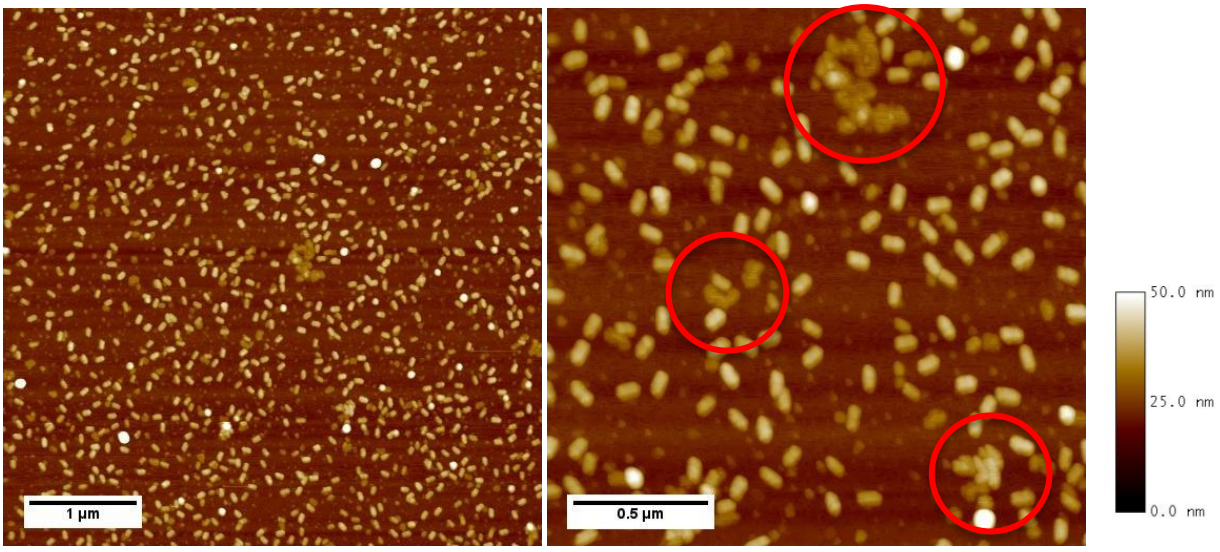

Figure 3.17 AFM images of AuNR-IgG protected with ZIF-8 after 48-hr incubation at 120 °C and rinsing of ZIF-8. ZIF-8 grew on the biosensor surface for 12 hr. Examples of deformed AuNR-IgG conjugates are highlighted in red circles.

3.5 Activity Preservation in Other Harsh Environments

Next we tested the activity preservation of these biosensors under exposure to organic solvents and proteolytic agents. Right after exposure to DMF for 2 hr, there was a blue shift of ~80 nm in the extinction spectra of the biosensors (Figure 3.18), indicating ZIF-8 film may be partially removed from the biosensor surface before the rinsing step. Still the unprotected biosensors retained 38% of their activity, while the biosensors with 12-hr of ZIF-8 growth had 68%, as shown in Figure 3.19. We also observed that exposure to DMF for longer time (3 hr) would cause complete loss of biosensor activity regardless of whether a ZIF-8 protective layer existed or not.

The silk fibroin, however, failed in protecting the plasmonic biosensors. After exposure to DMF for 2 hr, the samples only showed a 20-nm blue shift after rinsing, as shown in Figure 3.20 and Figure 3.21, which is minimal compared to the ~120-nm red shift after spin-coating of silk. This indicates that silk films could not remove from the biosensors surfaces after exposure to DMF. We also confirmed this hypothesis by AFM imaging. As shown in Figure 3.22, after rinsing the sample with nanopure water for 1 hr, the surface of the biosensor was still quite flat and we could not observe distinct AuNR-IgG conjugates in AFM scans.

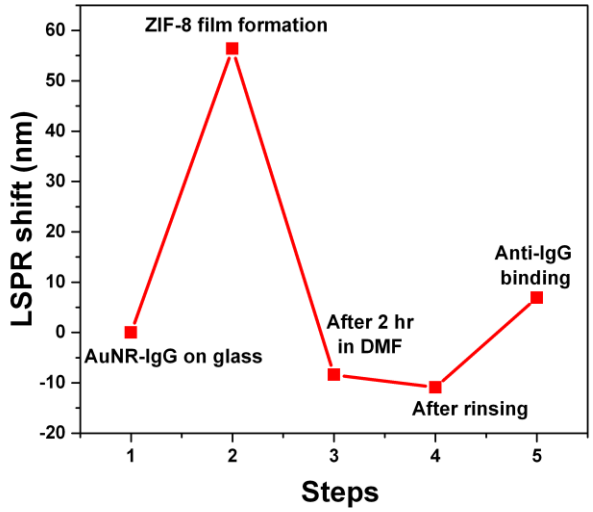

Figure 3.18 LSPR shifts of a plasmonic biosensor protected with ZIF-8 after ZIF-8 film formation for 12 hr, immersion in DMF for 2 hr, rinsing of ZIF-8 and anti-IgG binding.

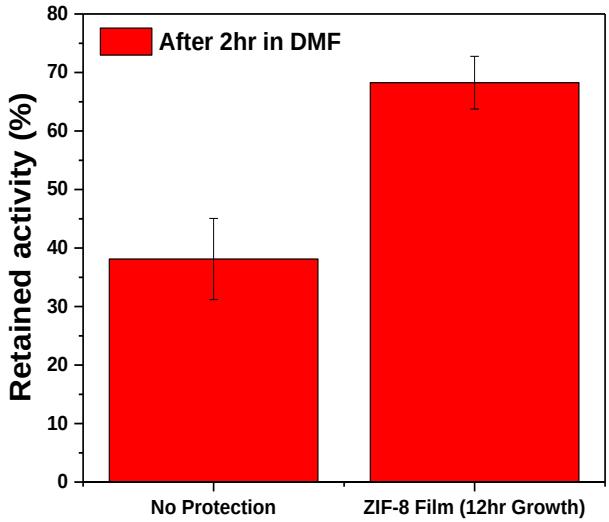

Figure 3.19 Retained activities of plasmonic biosensors after immersion in DMF for 2 hr (N ≥ 3 for each group). ZIF-8 grew on the biosensor surface for 12 hr.

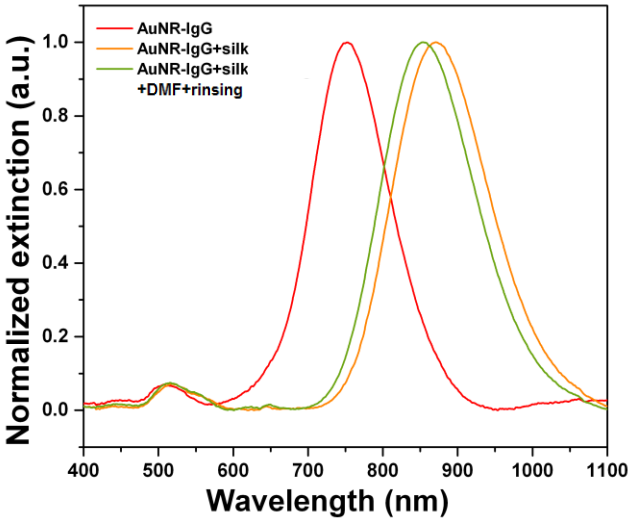

Figure 3.20 Extinction spectra of a plasmonic biosensor after deposition of silk film, and after immersion in DMF for 2 hr plus rinsing of silk.

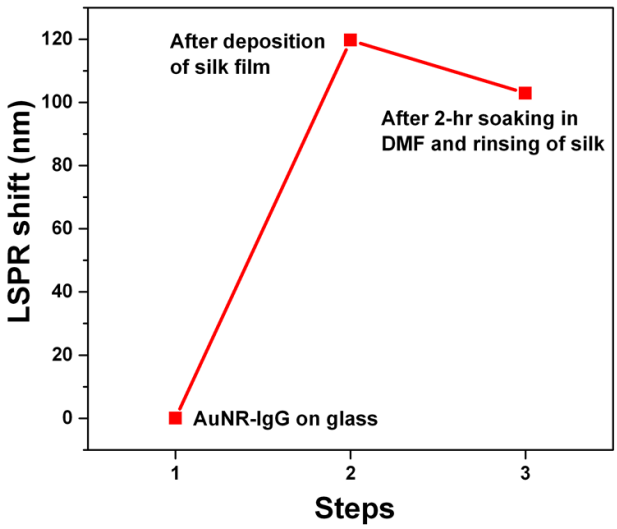

Figure 3.21 LSPR shifts of a plasmonic biosensor after deposition of silk film, and after immersion in DMF for 2 hr plus rinsing of silk.

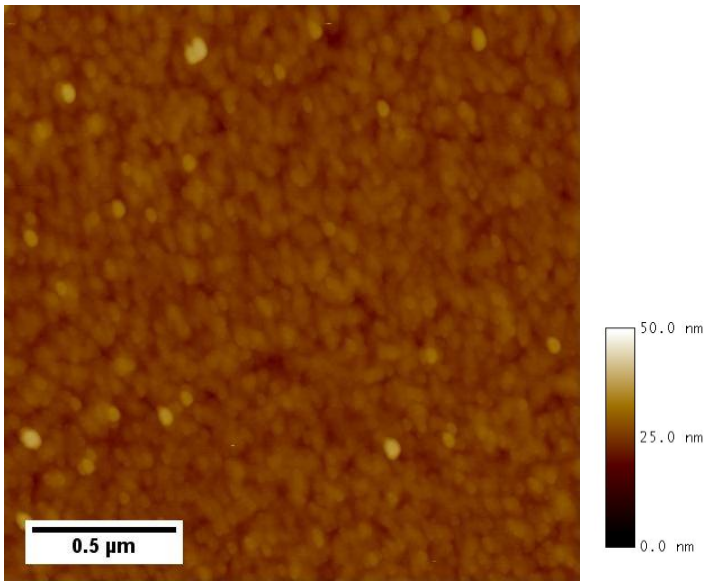

Figure 3.22 AFM image of a biosensor protected with silk fibroin film after immersion in DMF for 2 hr and rinsing of silk for 1 hr

A protease solution of 0.25 units/mL (Protease from *Streptomyces griseus*, Type XIV) was used to explore the effect of proteolytic agents. To protect the biosensors, ZIF-8 grew on the biosensors surfaces for 12 hr, and silk was spun-coated on biosensors surfaces for 60 sec at 3000 rpm. The LSPR shifts for protected and unprotected biosensors after each experimental step are shown in Figure 3.23. After exposure to protease solution for 2.5 hr, the unprotected samples showed a blue-shift after anti-IgG binding. Thus the retained activity can be treated as 0, as no successful binding of anti-IgG could be observed. The protected samples showed some red shift after anti-IgG binding. The average retained activities were 40% and 8% for samples protected with ZIF-8 and silk respectively ($N \geq 3$ for each group).

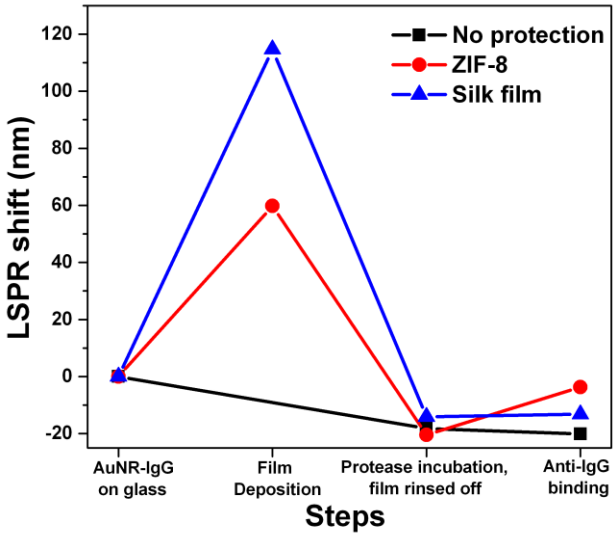

Figure 3.23 LSPR shifts of plasmonic biosensors with or without protective films after incubation in protease solution (0.25 units/mL) at 37°C for 2.5 hr.

We also noticed that after incubation in protease solutions and rinsing of protective layers, we can observe a blue shift in the longitudinal peak position compared to the initial value, as seen in Figure 3.23. This was not expected, and it may indicate a deformation of AuNR-IgG conjugates. To better understand this phenomenon, we scanned the biosensors with protective layers right after incubation in protease solution and very gentle rinsing. From Figure 3.24 we can see that as incubation time in protease solution increases, the outlines of ZIF-8 crystals became vague. After 2.5-hr incubation, we could hardly see any round ZIF-8 crystals similar as those in Figure 3.10. On

the other hand, the silk protective layer is completely removed after incubation in protease solution, as seen in Figure 3.25.

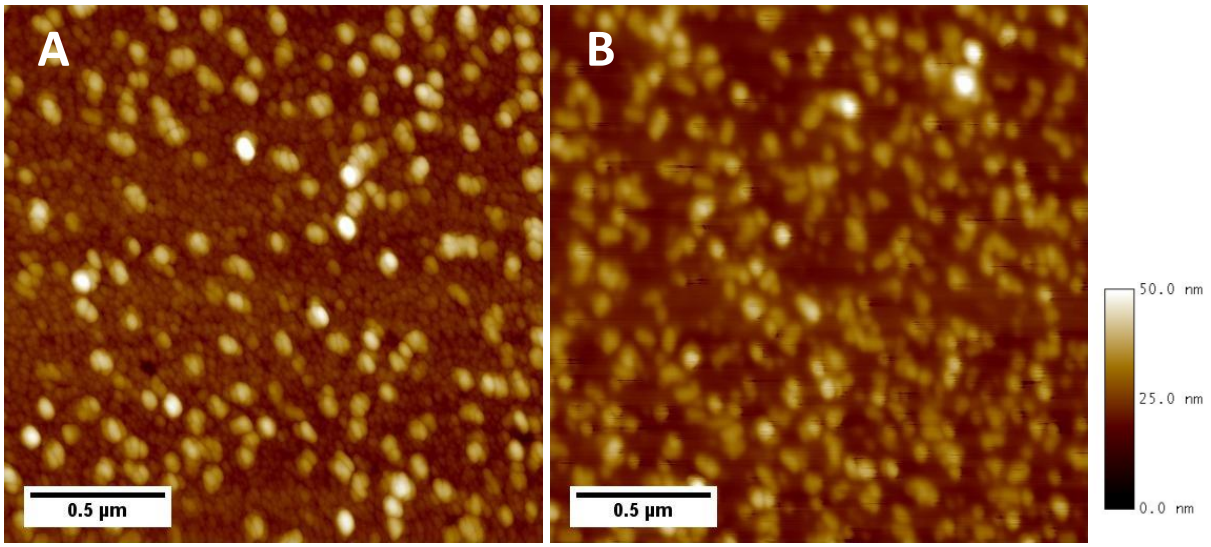

Figure 3.24 AFM images of biosensors protected with the same ZIF-8 film after incubation in protease solution (0.25 units/mL) at 37°C for different incubation times (A: 1 hr, B: 2.5 hr).

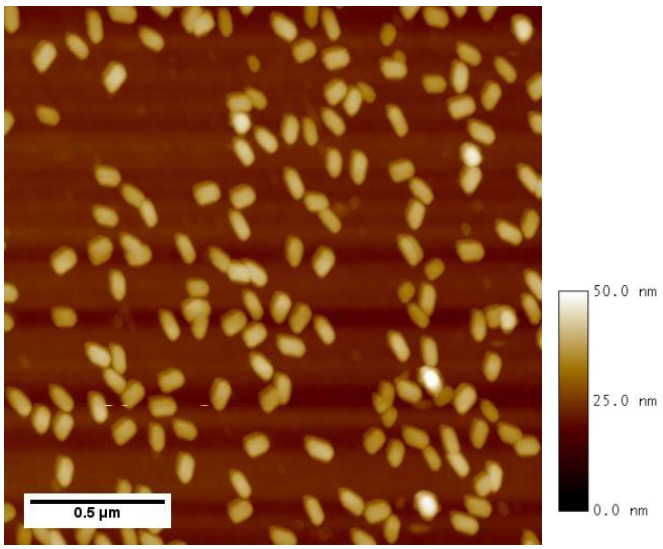

Figure 3.25 AFM image of a biosensor protected with silk after incubation in protease solution (0.25 units/mL) at 37°C for 2.5 hr.

Chapter 4

Discussion

ZIF-8 films showed the ability to preserve the activity of plasmonic biosensors, with their performance varying under different environmental conditions. This chapter will discuss the results from Chapter 3 in detail.

4.1 Plasmonic Biosensors

In this study, we fabricated plasmonic biosensors with IgG conjugated on AuNR, following a procedure similar to previously established methods [29,35,36]. Two batches of AuNRs with similar extinction peak values were used. The sizes of AuNRs used in this study are similar with the AuNR used in a previous study, with a larger aspect ratio and slightly larger standard deviation [35]. The difference in aspect ratio might attribute to the larger LSPR shift in extinction spectra after conjugation with SH-PEG-COOH, binding to anti-IgG and deposition of protective layers [37]. This can be related to the change in plasmon sensitivity. It has been reported that AuNRs with aspect ratios between 3 and 4 function better as plasmonic sensors. Therefore it is understandable that our AuNR with average aspect ratio of 3.9 would function better than the AuNR used in previous studies, which has an average aspect ratio of 2.8 [20,35,39]. In this case, the absolute values of signals from our plasmonic sensors, i.e. LSPR shifts, would be larger. However, the percent retained activity is always calculated with respect to a reference sample in the same batch. Therefore, the large absolute LSPR shift should not affect the assessment of efficiency for protective layers. Our data can be correlated with previous studies [35,36].

We verified the conjugation of SH-PEG-COOH on AuNRs with the change in extinction spectrum shown in Figure 3.2. The flexible PEG chains improved the accessibility of immobilized IgG, and the packed IgG layer reduced the potential nonspecific binding of proteins (including anti-IgG) on AuNRs surfaces, which can lead to errors in biosensor signals [16]. We observed a blue shift in the extinction spectra after AuNR-IgG conjugates adsorbed on the glass substrates. This shift is probably due to the significant change in refractive index of the environment [18]. From Figure 3.3,

we can see that AuNR-IgG conjugates were uniformly distributed on the glass substrates. Thus the extinction spectra obtained should reflect the average extinction from AuNR-IgG conjugates. Comparing Figure 3.3 and Figure 3.1, we can see that IgG conjugation did not greatly change the aspect ratio of the AuNRs, yet the shapes changed from simple rods to dumbbells. This was also observed in a previous study of plasmonic biosensors [35]. This may indicate preferential binding of SH-PEG-COOH at the two ends of an AuNR. Further investigation may proceed to understand the reason behind this phenomenon.

We characterized the function of plasmonic biosensors by LSPR shift after exposure to anti-IgG. To make signal from a sample biosensor comparable to that of its reference, we controlled the concentration of anti-IgG solution (24 μg/mL), as well as the exposure time in the same batch of biosensors. It has also been shown in a previous study that this concentration (24 μg/mL) of anti-IgG does not cause nonspecific binding of anti-IgG on bare AuNRs, and therefore we can attribute the LSPR shift to binding of anti-IgG to IgG [35].

4.2 Activity Preservation at Elevated Temperatures

ZIF-8 films successfully preserved the activity of the biosensors at various temperatures (40 °C, 60 °C and 80 °C), which satisfied our hypothesis that the porous and stable ZIF-8 crystals can protect biosensors at elevated temperatures. As the temperature increases, the retained activity of biosensors with ZIF-8 protection decreases. This may attribute to the thermal expansion of ZIF-8 increasing the pore size of the crystals, weakening the tight packing of crystals on IgG that makes activity preservation of antibodies possible [26,36]. While the retained activity of ZIF-8 protected plasmonic biosensors decreased at higher temperatures, the retained activity of control groups also lowered with increasing temperature. Thus more than 50% more of biosensor activity was retained with ZIF-8 at each temperature as discussed in Section 3.2.

Silk, however, failed to protect plasmonic biosensors at a relatively lower temperature of 80 °C for 24 hr. The insufficient LSPR shift associated with rinsing of silk film indicates incomplete removal of the silk films. This may be caused by silk fibers crystallizing, transforming from a water-soluble form (silk I) to insoluble β-sheets (silk II), making it hard to remove the protective silk films [42,43]. Further investigation may proceed to examine the protection of other antibody-based sensing systems with ZIF-8 crystals at extreme temperatures.

4.3 Progressive Growth of ZIF-8 Film

From Section 3.3, it is clear that the growth time of a ZIF-8 film can affect its preservation ability. With AFM images in Figure 3.10, we can see that uniform coverage is achieved in the case of all three growth times: 3 hr, 12 hr and 24 hr. No significant change in film roughness was observed from the AFM images for different growth times. The major difference in characteristics from the variation of growth time was the film thickness. Longer growth time results in thicker films, and better preservation of biosensor activities at an elevated temperature (80 °C).

This correlation may be caused by higher bulk-interface volume ratio for thicker materials. The preservation of biosensors activities is attributed to the small pore size of ZIF-8 and interactions between the carbonyl groups in protein backbone and the Zn cations of ZIF-8, providing proteins with tight encapsulation [26,36]. Therefore the interface between AuNR-IgG and ZIF-8 is mainly held by non-covalent interactions, which get substantially weaker at elevated temperatures. On the other hand, bulk ZIF-8 is thermally stable [23]. Thus, thicker rigid crystals may have provided better support to maintain the rigidity of interfacial regions.

Future investigations may proceed to understand the molecular basis of protein activity protection with ZIF-8 crystals.

4.4 Activity Preservation at Extremely High Temperature

At extremely high temperature of 120 °C, even though the temperature was not high enough to decompose ZIF-8 crystals, the blue shift in the extinction spectrum after removal of ZIF-8 indicates that the AuNR may have already deformed at this temperature, which would compromise the function of the plasmonic biosensors [23]. This is confirmed by the AFM images. The morphology of ZIF-8 did not show a significant change after incubation at 120 °C, yet the AuNR-IgG conjugates were clearly deformed. Some deformed AuNR-IgG conjugates showed that they might have been melted and re-joint together after cooling to room temperature. This phenomenon is coherent with previous studies in the thermal stability of AuNRs [40,41]. AuNRs can deform at temperatures much lower than the melting point of bulk gold to minimize its surface energy [41].

4.5 Activity Preservation in Other Harsh Environments

Compared to results in Section 3.2, the preserved activities of plasmonic biosensors are much lower in DMF and in protease solution, as shown in Section 3.4. The major reason behind this is probably dissociation of ZIF-8 in DMF and in water. Longer incubation time in either DMF or protease solution caused complete removal of ZIF-8 films from the biosensors surfaces. As the precursors of ZIF-8, zinc ions and 2-methylimidazole, may both exist in solution form in either DMF or water. Thus the stability of ZIF-8 may be lower in these media due to potential dissociation of the crystal. Silk fibroin films had an even poorer performance in DMF and protease solution. The failure in removing silk films after DMF treatments may attribute to the fact that silk crystallize into insoluble silk II form in some organic solvents [42,43].

Compared to the initial peak value, the blue shift after removal of ZIF-8 in protease solution was not expected. Since the biosensors retained some anti-IgG binding activity after removal of ZIF-8, this significant blue shift is probably due to the change of refractive index in the local environment, instead of the digestion of IgG. From the AFM images (Figure 3.24), we could see that in protease solution, the outline of ZIF-8 crystals gradually got vague. This may indicate that ZIF-8 is dissolving in protease solution, which may account for the unusual blue shift. Further research may be conducted to understand the reason why ZIF-8 crystals dissolve in protease solution at physiological pH. On the other hand, the low biosensor activity retained with silk in protease solution is understandable. Silk, being a protein itself, can naturally be digested by the protease solution, which contains several proteases targeting different positions in peptide chains. This is also supported by the AFM image (Figure 3.25).

One thing worth noting is that after incubation in protease solutions, the unprotected plasmonic sensors showed a blue shift in extinction spectra, followed by another blue shift after exposure to anti-IgG. This phenomena may be explained by the fact that protease from *Streptomyces griseus* targets some specific positions in peptide chains of proteins. Complete digestion of proteins is achieved sequentially. The first blue shift should be associated with the cleavage and initial decomposition of IgG on AuNRs, while the second blue shift may reflect further dissociation of IgG fragments from AuNRs. Since IgG is already digested by the proteases, it is unlikely that anti-IgG would bind on the AuNRs and cause a red shift.

4.6 ZIF-8 Film and Silk Fibroin Film

As discussed in Sections 4.2 and 4.3, ZIF-8 films proved to be a great material for activity preservation of plasmonic biosensors at elevated temperatures. Comparing Figure 3.3 and Figure 3.7, we can see that the shape and distribution of AuNR-IgG conjugates on the surfaces of plasmonic sensors had not changed much during the formation and rinsing of ZIF-8 film. In previous studies, both silk fibroin films and ZIF-8 films successfully retained, with over 70% of retained activity reported for AuNR-IgG based biosensors at room temperature after 7 days [35,36]. Therefore we expected them to show similar preservation of biosensors in this study. Yet comparing the results of ZIF-8 films and silk fibroin films in Sections 3.2 and 3.4, ZIF-8 films show a significantly better preservation at elevated temperatures, in an organic solvent and in a protease solution. This may be partially due to the potential transformation of silk film from water-soluble Silk I to insoluble Silk II under various conditions, as discussed in Sections 4.2 and 4.4. Also silk is a protein just like the antibodies, which means silk would be unstable when exposed to proteolytic substances.

We also noticed that ZIF-8 films showed better preservation ability at elevated temperatures than in protease solutions. This is probably because we did the temperature treatments with low humidity. Both ZIF-8 films and silk fibroin films cannot effectively protect the plasmonic biosensors in aqueous environments. ZIF-8 is not stable in aqueous solutions, especially at low pH [36]. Silk fibroin films may stay on the sensor surfaces longer due to its sticky nature. However, amorphous silk I can still dissolve in water, while crystallized silk II films are stable in solutions and very hard to remove. These phenomena may contribute to the fact that preserved activities for both films are much higher in dry conditions [35]. The protection ability of both methods may be impaired by a change in humidity. In dry conditions, ZIF-8 is a great material for protecting plasmonic biosensors.

4.7 Activity Preservation of Plasmonic Biosensors

With ZIF-8 films, we can successfully preserve the activity of antibody-based plasmonic biosensors at elevated temperatures in dry environments. This preservation procedure is not only energy-efficient, but also easy to operate. Thus, it can largely expand the potential applications of these plasmonic biosensors in resource-limited settings such as urban and rural clinics, developing countries with low-moderate incomes, and disaster struck regions where refrigeration and electricity may not be accessible. Similarly, we can possibly use ZIF-8 to protect other biological substances that are susceptible to changes in temperature, such as clinical samples, vaccines and medicines. Future researches may proceed in this direction.

Chapter 5

Conclusions

In this study, we investigated a new method of activity preservation for antibody-based plasmonic biosensors using ZIF-8 films. ZIF-8 films can successfully grow on the biosensors, protect the biosensor activity in various conditions, and easily get removed before analyte detection. With ZIF-8 films, the biosensors can retain 50% more of their activity than the unprotected cases at elevated temperatures of 40 °C, 60°C and 80 °C. At 40 and 60 °C, around 80% of the biosensors activities can be retained. With longer growth time for ZIF-8 crystals, thicker films form on the plasmonic biosensors, and their preservation abilities improve. By increasing the growth time from 3 hr to 24 hr, the average retained activity of plasmonic biosensors at 80 °C can improve from 60% to 78%. This preservation is lost at an extremely high temperature of 120 °C due to the instability of AuNRs. Activity preservation of plasmonic biosensors using ZIF-8 was also explored in an organic solvent (DMF) and a proteolytic agent (protease from *Streptomyces griseus*). However, ZIF-8 crystals tend to dissolve in these two conditions, which limit its activity preservation to a very short period. Further investigation may proceed to understand the reason behind the instability of ZIF-8 films in these two environments. Still ZIF-8 films show a greater capability of activity preservation for antibody-based biosensors than silk fibroin films in all three kinds of harsh conditions: at high temperatures, in an organic solvent and in a protease solution.

Further study may proceed to investigate the preservation of protein or antibody function using ZIF-8 crystals in other environments such as UV radiation and sonication, and the mechanism behind this activity preservation.

References

[1] Endo, Tatsuro, et al. "Multiple label-free detection of antigen-antibody reaction using localized surface plasmon resonance-based core-shell structured nanoparticle layer nanochip." Analytical Chemistry 78.18 (2006): 6465-6475.

[2] Anker, Jeffrey N., W. Paige Hall, Olga Lyandres, Nilam C. Shah, Jing Zhao, and Richard P. Van Duyne. "Biosensing with plasmonic nanosensors." Nature Materials 7, no. 6 (2008): 442-453.

[3] Zhang, Jeney, Eleanor Pritchard, Xiao Hu, Thomas Valentin, Bruce Panilaitis, Fiorenzo G. Omenetto, and David L. Kaplan. "Stabilization of vaccines and antibiotics in silk and eliminating the cold chain." Proceedings of the National Academy of Sciences 109, no. 30 (2012): 11981-11986.

[4] Widmaier, Eric P., Hershel Raff, and Kevin T. Strang. "Chapter 18: The Immune System." In Vander's Human Physiology: The Mechanisms of Body Function, 662-85. 13th ed. Boston, MA: McGraw-Hill, 2013.

[5] Janeway Jr, Charles A., Paul Travers, Mark Walport, and Mark J. Shlomchik. "The interaction of the antibody molecule with specific antigen." (2001).

[6] Vilím, Vladimír, Zdeněk Vobůrka, Richard Vytásek, Ladislav Senolt, Ilja Tchetverikov, Virginia B. Kraus, and Karel Pavelka. "Monoclonal antibodies to human cartilage oligomeric matrix protein: epitope mapping and characterization of sandwich ELISA." Clinica chimica acta; international journal of clinical chemistry 328, no. 1-2 (2003): 59-69.

[7] Ashley, Rhoda L., Julie Militoni, Francis Lee, Andre Nahmias, and Lawrence Corey. "Comparison of Western blot (immunoblot) and glycoprotein G-specific immunodot enzyme assay for detecting antibodies to herpes simplex virus types 1 and 2 in human sera." Journal of Clinical Microbiology 26, no. 4 (1988): 662-667.

[8] Shimizu, Makoto, Hitoshi Nagashima, Keisuke Sano, Kei Hashimoto, Makoto Ozeki, Ken Tsuda, and Hajime Hatta. "Molecular stability of chicken and rabbit immunoglobulin G." Bioscience, biotechnology, and biochemistry 56, no. 2 (1992): 270-274.

[9] Russell, Alan J., Laura J. Trudel, Paul L. Skipper, John D. Groopman, Steven R. Tannenbaum, and Alexander M. Klibanov. "Antibody-antigen binding in organic solvents." Biochemical and biophysical research communications 158, no. 1 (1989): 80-85.

[10] Auriault, C., M. A. Ouaissi, G. Torpier, H. Eisen, and A. Capron. "Proteolytic cleavage of IgG bound to the Fc receptor of Schistosoma mansoni schistosomula." Parasite Immunology 3, no. 1 (1981): 33-44.

[11] Wolfson, Lara J., François Gasse, Shook-Pui Lee-Martin, Patrick Lydon, Ahmed Magan, Abdelmajid Tibouti, Benjamin Johns, Raymond Hutubessy, Peter Salama, and Jean-Marie Okwo-Bele. "Estimating the costs of achieving the WHO-UNICEF Global Immunization Vision and Strategy, 2006-2015." Bulletin of the World Health organization 86, no. 1 (2008): 27-39.

[12] Willets, Katherine A., and Richard P. Van Duyne. "Localized surface plasmon resonance spectroscopy and sensing." Annu. Rev. Phys. Chem. 58 (2007): 267-297.

[13] Brockman, Jennifer M., Bryce P. Nelson, and Robert M. Corn. "Surface plasmon resonance imaging measurements of ultrathin organic films." Annual review of physical chemistry 51, no. 1 (2000): 41-63.

[14] Berger, Charles EH, Tom AM Beumer, Rob PH Kooyman, and Jan Greve. "Surface plasmon resonance multisensing." Analytical Chemistry 70, no. 4 (1998): 703-706.

[15] Mayer, Kathryn M., and Jason H. Hafner. "Localized surface plasmon resonance sensors." Chemical reviews 111, no. 6 (2011): 3828-3857.

[16] Tian, Limei, Jeremiah J. Morrissey, Ramesh Kattumenu, Naveen Gandra, Evan D. Kharasch, and Srikanth Singamaneni. "Bioplasmonic paper as a platform for detection of kidney cancer biomarkers." Analytical chemistry 84, no. 22 (2012): 9928-9934.

[17] Huang, Xiaohua, Svetlana Neretina, and Mostafa A. El ‐ Sayed. "Gold nanorods: from synthesis and properties to biological and biomedical applications." Advanced Materials 21, no. 48 (2009): 4880-4910.

[18] Tian, Limei, Enze Chen, Naveen Gandra, Abdennour Abbas, and Srikanth Singamaneni. "Gold nanorods as plasmonic nanotransducers: distance-dependent index sensitivity." Langmuir 28, no. 50 (2012): 17435-17442.

[19] Becker, Jan, Andreas Trügler, Arpad Jakab, Ulrich Hohenester, and Carsten Sönnichsen. "The optimal aspect ratio of gold nanorods for plasmonic bio-sensing." Plasmonics 5, no. 2 (2010): 161-167.

[20] Kitagawa, Susumu, Ryo Kitaura, and Shin ‐ ichiro Noro. "Functional porous coordination polymers." Angewandte Chemie International Edition 43, no. 18 (2004): 2334-2375.

[21] Yaghi, Omar M., Michael O'Keeffe, Nathan W. Ockwig, Hee K. Chae, Mohamed Eddaoudi, and Jaheon Kim. "Reticular synthesis and the design of new materials." Nature 423, no. 6941 (2003): 705-714.

[22] Bux, Helge, Fangyi Liang, Yanshuo Li, Janosch Cravillon, Michael Wiebcke, and Jürgen Caro. "Zeolitic imidazolate framework membrane with molecular sieving properties by

microwave-assisted solvothermal synthesis." Journal of the American Chemical Society 131, no. 44 (2009): 16000-16001.

[23] Park, Kyo Sung, Zheng Ni, Adrien P. Côté, Jae Yong Choi, Rudan Huang, Fernando J. Uribe-Romo, Hee K. Chae, Michael O'Keeffe, and Omar M. Yaghi. "Exceptional chemical and thermal stability of zeolitic imidazolate frameworks." Proceedings of the National Academy of Sciences 103, no. 27 (2006): 10186-10191.

[24] Zhuang, Jia, Chun-Hong Kuo, Lien-Yang Chou, De-Yu Liu, Eranthie Weerapana, and Chia-Kuang Tsung. "Optimized metal–organic-framework nanospheres for drug delivery: evaluation of small-molecule encapsulation." ACS nano 8, no. 3 (2014): 2812-2819.

[25] Liang, Kang, Raffaele Ricco, Cara M. Doherty, Mark J. Styles, Stephen Bell, Nigel Kirby, Stephen Mudie et al. "Biomimetic mineralization of metal-organic frameworks as protective coatings for biomacromolecules." Nature communications, 6 (2015).

[26] Feng, Yi, Asher Schmidt, and R. A. Weiss. "Compatibilization of polymer blends by complexation. 1. Spectroscopic characterization of ion-amide interactions in ionomer/polyamide blends." Macromolecules 29, no. 11 (1996): 3909-3917.

[27] McEldoon, James P., and Jonathan S. Dordick. "Unusual thermal stability of soybean peroxidase." Biotechnology progress 12, no. 4 (1996): 555-558.

[28] Angenendt, Philipp, Jörn Glökler, Derek Murphy, Hans Lehrach, and Dolores J. Cahill. "Toward optimized antibody microarrays: a comparison of current microarray support materials." Analytical biochemistry 309, no. 2 (2002): 253-260.

[29] Tadepalli, Sirimuvva, Zhifeng Kuang, Qisheng Jiang, Keng-Ku Liu, Marilee A. Fisher, Jeremiah J. Morrissey, Evan D. Kharasch, Joseph M. Slocik, Rajesh R. Naik, and Srikanth Singamaneni. "Peptide Functionalized Gold Nanorods for the Sensitive Detection of a Cardiac Biomarker Using Plasmonic Paper Devices." Scientific reports 5 (2015).

[30] Rockwood, Danielle N., Rucsanda C. Preda, Tuna Yücel, Xiaoqin Wang, Michael L. Lovett, and David L. Kaplan. "Materials fabrication from Bombyx mori silk fibroin." Nature protocols 6, no. 10 (2011): 1612-1631.

[31] Hakimi, Osnat, David P. Knight, Fritz Vollrath, and Pankaj Vadgama. "Spider and mulberry silkworm silks as compatible biomaterials." Composites Part B: Engineering 38, no. 3 (2007): 324-337.

[32] Yucel, Tuna, Michael L. Lovett, and David L. Kaplan. "Silk-based biomaterials for sustained drug delivery." Journal of Controlled Release 190 (2014): 381-397.

[33] Tao, Hu, David L. Kaplan, and Fiorenzo G. Omenetto. "Silk materials–a road to sustainable high technology." Advanced materials 24, no. 21 (2012): 2824-2837.

[34] Zhou, Cong, Zhao, Fabrice Confalonieri, Michel Jacquet, Roland Perasso, Zhen‐Gang Li, and Joel Janin. "Silk fibroin: structural implications of a remarkable amino acid sequence." Proteins: Structure, Function, and Bioinformatics 44, no. 2 (2001): 119-122.

[35] Wang, Congzhou, Jingyi Luan, Sirimuvva Tadepalli, Keng-Ku Liu, Jeremiah J. Morrissey, Evan D. Kharasch, Rajesh R. Naik, and Srikanth Singamaneni. "Silk-Encapsulated Plasmonic Biochips with Enhanced Thermal Stability." ACS Applied Materials & Interfaces 8, no. 40 (2016): 26493-26500.

[36] Wang, Congzhou, Sirimuvva Tadepalli, Jingyi Luan, Keng-Ku Liu, Jeremiah J. Morrissey,3, Evan D. Kharasch, Rajesh R. Naik and Srikanth Singamaneni, "Metal-Organic Framework as Protective Coating for Biodiagnostic Chips." Working paper, Department of Mechanical Engineering and Materials Science, Washington University, St. Louis, 2016.

[37] Lee, Kyeong-Seok, and Mostafa A. El-Sayed. "Dependence of the enhanced optical scattering efficiency relative to that of absorption for gold metal nanorods on aspect ratio, size, end-cap shape, and medium refractive index." The Journal of Physical Chemistry B 109, no. 43 (2005): 20331-20338.

[38] Zhu, Minqi, Jacek B. Jasinski, and Moises A. Carreon. "Growth of zeolitic imidazolate framework-8 crystals from the solid–liquid interface." Journal of Materials Chemistry 22, no. 16 (2012): 7684-7686.

[39] Link, Stephan, M. B. Mohamed, and M. A. El-Sayed. "Simulation of the optical absorption spectra of gold nanorods as a function of their aspect ratio and the effect of the medium dielectric constant." The Journal of Physical Chemistry B 103, no. 16 (1999): 3073-3077.

[40] Wang, Yanting, S. Teitel, and Christoph Dellago. "Surface-driven bulk reorganization of gold nanorods." Nano letters 5, no. 11 (2005): 2174-2178.

[41] Petrova, Hristina, Jorge Perez Juste, Isabel Pastoriza-Santos, Gregory V. Hartland, Luis M. Liz-Marzán, and Paul Mulvaney. "On the temperature stability of gold nanorods: comparison between thermal and ultrafast laser-induced heating." Physical Chemistry Chemical Physics 8, no. 7 (2006): 814-821.

[42] Gupta, Maneesh K., Srikanth Singamaneni, Michael McConney, Lawrence F. Drummy, Rajesh R. Naik, and Vladimir V. Tsukruk. "A facile fabrication strategy for patterning protein chain conformation in silk materials." Advanced Materials 22, no. 1 (2010): 115-119.

[43] Jin, Hyoung-Joon, and David L. Kaplan. "Mechanism of silk processing in insects and spiders." Nature 424, no. 6952 (2003): 1057-1061.

Vita

Lu Wang

Degrees	M.S. Materials Science, December 2016 B.S. Biomedical Engineering, December 2016
Professional Societies	Alpha Eta Mu Beta National Biomedical Engineering Society Tau Beta Pi Engineering Honor Society

December 2016